UNIVERSIDADE DE LISBOA
FACULDADE DE CIÊNCIAS
DEPARTAMENTO DE QUÍMICA E BIOQUÍMICA

Characterization of Voltage-Gated Potassium Channels from Dorsal Root Ganglia Neurons in Neuropathic and Inflammatory Chronic Pain

Beatriz Szwarc dos Santos

Mestrado em Bioquímica
Especialização em Bioquímica Médica

Dissertação orientada por:
Prof. Dr. Pedro Afonso dos Santos Baltazar de Lima

2017

ACKNOWLEDGEMENTS

Ao meu orientador, Doutor Pedro Lima, por, no meu último ano de licenciatura, ter enaltecido o poder das ideias e de correr atrás delas. Desde então, vontade e entusiasmo são palavras de ordem, e por isso também, obrigada por dar espaço para abrir as asas e questionar acerca de tudo e de nada, até surgir uma ideia. Um grande obrigada me ter oferecido um lugar no seu laboratório, por me ter alimentado o bichinho da neurociência e por ter acompanhado todos os passos de perto, sempre com uma mão estendida pronta a ajudar. Obrigada pela descoberta da electrofisiologia e pela descoberta de um grupo de investigação tão porreiro como o nosso.

À minha co-orientadora não-oficial e amiga, Joana. Obrigada, Joana! Pela paciência, pelos ensinamentos, pelos rolares de olhos e pelas gargalhadas. Obrigada pelos brainstorms e obrigada pelos "TPCs". Obrigada por saberes quando apertar comigo e quando deixar andar. Obrigada por tudo. Esta tese é muito graças a ti.

Ao André, a pessoa que me deu a conhecer o amplificador, as pipetas e os eléctrodos. Mais que isso, a pessoa que todos os dias trouxe um sorriso consigo para o laboratório. E que nunca deixou de dar uma palavra amiga, um abraço e uma ajuda. Obrigada por toda a ajuda, por toda a alegria e pelo bom apetxitxi.

À Clara um grande, grande obrigada. Seja pelo ananás no dia do empurrão final, seja pelo sorriso animador, pronto a sair *on demand*.

À Marisa, por sempre se disponibilizar a ajudar, por pegar numa cadeira e discutir resultados.

Finalmente, mas não por fim, um grande obrigada Mãe e Pai. Obrigada por apoiarem todos os meus estudos, por apoiarem todos os meus sonhos, por me ampararem quando caio e por me desafiarem quando estagno. Obrigada pelo vosso amor e carinho.

Ao meu irmão, Pedro. Obrigada por seres sempre capaz pôr tudo em perspectiva, obrigada pelos cimocerróides e camarões pistola. Obrigada pelo teu amor e carinho.

Aos meus avós, à Ósa, à Bel e ao Vô, que sempre celebraram todas as minhas vitórias como deles. Obrigada pelo vosso amor e carinho.

Obrigada Zé, obrigada por nunca me deixares baixar os braços nem desanimar. Obrigada pelo teu amor e carinho.

Não poderia deixar de agradecer à Tia Maria. Obrigada pela voz doce que sempre me encorajou a seguir o coração e a ciência.

TABLE OF CONTENTS

ABBREVIATIONS

ATP	Adenosine triphosphate
BDNF	Brain-derived Neurotrophic Factor
BSA	Bovine Serum Albumin
Ca^{2+}	Calcium ion
CCI	Chronic Constriction Injury
CFA	Complete Freund's adjuvant
Cm	Whole-cell membrane Capacitance
CNS	Central Nervous System
DRG	Dorsal Root Ganglion
DTT	Dithiothreitol
FBS	Fetal Bovine Serum
G	Conductance
HB	Homogeneization Buffer
I	Current amplitude
IASP	International Association for the Study of Pain
IB4	Isolectin 4
I-V	Current-Voltage relationship
J	Current Density
K^+	Potassium ion
Kv	Voltage-gated Potassium Channel
L	Lumbar
LB	Lysis Buffer
mRNA	Messenger Ribonucleic Acid

Na^+	Sodium ion
Nav	Voltage-gated Sodium Channel
NGF	Neurotrophic Growth Factor
PBS	Phosphate Buffered Saline
PIC	Protease Inhibitor Cocktail
PNS	Peripheral Nervous System
RMP	Rest Membrane Potential
Rpm	Rotations per minute
S	Sacral
SDS	Sodium dodecyl sulphate
SEM	Standard Error of the Mean
SNL	Spared Nerve Ligation
TrkA	Tropomyosin receptor kinase A
TRP	Transient Receptor Potential Channel
TRPA	Transient Receptor Potential Channel, sub-family A - Ankyrin
TRPM	Transient Receptor Potential Channel, sub-family M -Melastin
TRPV	Transient Receptor Potential Channel, sub-family V -Vanilloid
TTX	Tetrodotoxin
V_H	Voltage of half activation or inactivation
vFF	von Frey Filament
Vm	Voltage pulsed current
V_S	Slop constant
τ	Time constant

RESUMO

Dor crónica afeta 21% da população humana e, até à data, os tratamentos disponíveis são apenas parcialmente eficazes. Esta condição resulta, muitas vezes, em perturbação de sono, desenvolvimento de depressão e ansiedade que prejudicam a qualidade de vida dos pacientes. Uma das formas mais incapacitantes da dor crónica é a dor neuropática, resultante de lesões nos nervos sensoriais. Existem muitas outras etiologias de dor crónica como por exemplo a inflamatória (artrite reumática) e a neuropática diabética. Em dor crónica, os doentes sofrem de hiperalgesia (reação exagerada a um estímulo doloroso), alodínia (sensação de dor a um estímulo não doloroso), dor espontânea, parestesia (sensação anormal) e disestesia (parestesia desconfortável). A dor crónica é especialmente difícil de tratar muito porque não se compreende totalmente os mecanismos moleculares que a causam. Atualmente, o tratamento da dor crónica continua a ser um desafio pois a maioria dos alvos das atuais abordagens terapêuticas coexistem no sistema nervoso central e, por isso, promovem vários efeitos colaterais tais como dependência e habituação.

As fibras sensoriais que são responsáveis pela transmissão de estímulos de dor (fibras C e Aδ) encontram-se num estado mais elevado de hiperexcitabilidade numa situação de dor crónica. Tal excitação é controlada por um conjunto de canais iónicos ativados por voltagem (entre outros) que produzem um grau de excitação que é, numa situação normal, proporcional à intensidade do estímulo externo. No contexto de nervo sensorial danificado, este torna-se hiperativo e produz atividade elétrica espontânea que o cérebro interpreta como sinais de dor. Tal pode se traduzir numa situação de dor crónica, onde a coordenação é interrompida, resultando em excitabilidade periférica desregulada.

A velocidade de transmissão nas fibras C é mais lenta relativamente à velocidade de transmissão das fibras Aδ devido à ausência de um revestimento de mielina. Desta forma, a perceção dos estímulos transmitidos pelas fibras C é mais difusa que das fibras Aδ. As fibras sensoriais primárias ou nocicetivas são constituídas pelos neurónios do gânglio da raiz dorsal (DRG, do inglês *Dorsal Root Ganglia*). Os neurónios DRG de pequeno diâmetro apresentam uma atividade aumentada em pacientes com dor crónica, e por isso serão o foco desta dissertação.

Na presença de estímulos capazes de produzir dor (ou seja, cuja magnitude é superior ao limiar de ativação das fibras nervosas) os recetores nas terminações nervosas dos neurónios primários são ativados, despolarizando a membrana e produzindo um potencial

de ação. Esta despolarização propaga-se pela fibra nervosa, sendo o sinal transmitido para os neurónios secundários e sistema nervoso central onde, no córtex sensorial do cérebro, a informação a relativa à quantificação e localização da dor é integrada.

O papel dos canais de K^+ no controlo do potencial de repouso da membrana, no limiar de disparo, frequência e forma do potencial de ação é crucial. Estudos indicam que a inibição dos canais de K^+ induz a atividade espontânea em fibras sensoriais periféricas, cuja hiperexcitabilidade em estados de dor crónica coincidiu com a sua regulação negativa. Assim, a supressão da condutância de K^+ pode representar uma condição geral de um nervo 'doloroso'. A diminuição da atividade dos canais de K^+ ativados por voltagem faz parte de um mecanismo geral para a hiperneuroexcitabilidade periférica em dor crónica, e que potenciadores destes canais podem significar um melhoramento desta doença.

O objetivo do trabalho experimental foi a elucidação dos mecanismos comuns e específicos de dor crónica com origem neuropática e inflamatória em modelos de ratos. A compreensão da base mecanística do mau funcionamento de canais de K^+ ativados por voltagem (Kv) em termos de localização, biofísica, e consequências para a neurotransmissão é uma potencial de novas terapias para a dor. Especificamente, foi estudada a biofísica de canais Kv em neurónios de DRG de pequeno diâmetro.

Sabendo que a dor crónica pode ter várias etiologias, este projeto focou-se na dor crónica de origem inflamatória e neuropática, baseando-se em modelos animais de dor em ratos. A dor crónica neuropática foi estudada com base no modelo *Chronic Constriction Injury* (CCI) que assenta na constrição crónica do nervo isquiático do rato através de quatro nós soltos. A dor crónica inflamatória foi estudada através da indução de monoartrite no joelho do rato, pela injeção de uma substância que ativa o sistema imunitário: *Complete Freund's Adjuvant* (CFA).

O desenvolvimento de dor crónica foi acompanhado por testes comportamentais que incluem a medição de sensibilidade mecânica e de atividade vertical. Ao fim de 4 semanas (para CCI) e de 2 semanas (para CFA), os ratos foram sacrificados por decapitação após anestesia com pentobarbital para análise dos neurónios DRG de pequeno diâmetro por eletrofisiologia.

No modelo neuropático CCI, os ratos modelo desenvolveram hiperalgesia durante o curso da experiência mantendo-a sempre abaixo dos respetivos controlos. No modelo inflamatório CFA foi observada inicialmente uma maior sensibilidade após a indução do

modelo, evoluindo para uma recuperação total da sensibilidade no final do tempo do modelo.

Resultados de *whole-cell voltage-clamp* demonstram que a dor crónica altera as propriedades biofísicas das correntes dos canais de K^+ ativados por voltagem. Especificamente, ambos os modelos CCI e CFA partilham um mecanismo relativo à redução da componente rápida das correntes de K^+.

O modelo de dor crónica neuropática mostra ainda um mecanismo específico subjacente de aumento da componente lenta das correntes de K^+. Os ensaios proteicos revelaram uma expressão aumentada de Kv1.3 (uma isoforma de canais de K^+ ativados por voltagem), a qual aparenta ser responsável por este aumento da componente lenta.

O modelo de dor crónica inflamatória mostra uma alteração específica relativa a uma despolarização do perfil de ativação da componente rápida das correntes de K^+, sugerindo uma alteração de sensibilidade à voltagem para valores mais despolarizados.

No seu conjunto, os dados apontam para a identificação de componentes da corrente de K^+ que estão diferencialmente expressas nos modelos de dor crónica. Esta informação em combinação com os ensaios de expressão proteica sugerem a identificação molecular das componentes da corrente de K^+.

Os resultados conseguidos durante esta tese de mestrado trouxeram novos conhecimentos para a validação de alvos dor moleculares terapêuticos e para a identificação de novas abordagens experimentais / terapêuticas para dor neuropática e inflamatória, bem como o seu mecanismo de ação, que continuará a ser explorado pelo laboratório.

Palavras-chave: Dor crónica; canais de potássio dependentes de voltagem; gânglios da raiz dorsal.

ABSTRACT

Chronic pain affects 21% of the human population and, to date, standard treatments are only partially effective. This condition often results in poor sleep, depression and anxiety, between other, which highly impair patients' quality of life. One of the most disabling forms of chronic pain is called neuropathic pain, which results from injuries to sensory nerves. Pain or discomfort is felt in response to non-painful stimuli. Chronic pain is difficult to treat as currently we do not fully understand the associated molecular mechanisms.

Stimulating a nerve above the threshold of activation causes it to produce action potentials. Neurotransmission follows action potentials which are generated by ions moving into and out of the neuronal-membrane through voltage-gated ionic channel. Voltage-gated sodium and potassium channels (Nav and Kv, respectively) are critical to the generation of these action potentials that convey nociceptor signals to synapses in the dorsal horn. In this context, nociceptive fibers that are responsible for the transmission of pain stimuli are in a higher state of excitability with pain. Such excitation is controlled by an intricate set of ion channels that are coordinated to produce a degree of excitation that, in a naïve situation, is proportional to the strength of the external stimulation. Once a sensory nerve is damaged or injured it becomes hyperactive and produces spontaneous electrical activity that the brain interprets as pain signals. In chronic pain coordination by ion channels is disrupted, resulting in deregulated peripheral excitability. Of those sensory fibers, small diameter dorsal root ganglia (DRG) neurons are found to have an augmented activity in chronic pain patients. There is strong evidence that modulation of specific Na^+, Calcium (Ca^{2+}) or K^+ channel sub-types can be effective in treating chronic pain, although there is still no modulator on the clinical setting specifically targeting those channels expressed in pain-sensing neurons from DRG. Moreover, it is not fully understood how chronic pain affects the ion channel dynamics in a way that generates this hyperactivity.

The goal of the present work was to elucidate shared and specific mechanisms of neuropathic and inflammatory chronic pain involving K^+ channels, using pain rat models. Understanding the mechanistic basis of ion channel malfunction in terms of trafficking, localization, biophysics, and consequences for neurotransmission is a potential route to new pain therapies. Specifically, we studied the biophysics of voltage activated K^+ currents and underlying Kv channels in small diameter DRG neurons and determine routes of pharmacological modulation of these currents as a strategy for new analgesic drug design.

Knowing that chronic pain can have several etiologies, this project focused on chronic pain of neuropathic and inflammatory origin, based on rat models of pain. Chronic neuropathic pain was studied based on *Chronic Constriction Injury* (CCI) , which is based on the chronic constriction of the rat sciatic nerve through four loose ligation Chronic inflammatory pain was studied through the induction of monoarthritis in the knee of the rat by the injection of a substance that activates the immune system: *Complete Freund's Adjuvant* (CFA).

The pain models were followed with behavioral tests that included the measurement of mechanical sensitivity and vertical activity. After 4 weeks (for the CCI) and 2 weeks (for the CFA model), rats were sacrificed and their DRG removed aiming the electrophysiological analysis from small diameter DRG neurons.

In the neuropathic CCI model, the model rats developed hyperalgesia during the experiment, keeping their threshold for pain below the respective controls. In the inflammatory CFA model, a greater sensitivity was observed by the third day after model induction, progressing to a full recovery of sensitivity at the end of the model time.

Whole-cell voltage-clamp results demonstrated that chronic pain alters the biophysical properties of voltage-activated K^+ channel currents. Importantly, both CCI and CFA models share a mechanism, a reduction of the fast component of K^+ current (I_{fast}, an A-type current).

The neurons from the CCI pain model also showed a specific current output: an increase of current density of the slow K^+ current component (I_{slow}). Western-blot protein assays revealed over expression of Kv1.3, which may be responsible for this increase in I_{slow}.

In terms of channel gating phenomena, neurons from CFA rats showed a specific biophysical alteration – in relation to neurons from naïve rats, the voltage dependence of activation showed more depolarized curves. Finally, in terms of the voltage dependence of steady-state inactivation, neurons from both pain rat models exhibited more depolarized voltage profiles. Such impairment of the inactivation is concordant with the alleged increase excitability in damaged neurons.

Taken together, the data reveals mechanisms underlying increases in neuroexcitability which lead to neuronal hyperactivity and hyperalgesia. The results also points to the identification of specific and shared phenomena occurring in K^+ current components that are differentially expressed in the pain models. This information, together

with the protein expression assays, suggest the molecular identification of the K^+ current-component.

The results obtained during this master's thesis bring new knowledge about the therapeutic molecular pain targets and for the identification of new experimental / therapeutic approaches for neuropathic chronic pain and inflammatory pain, as well as its underlying mechanisms, which will continue to be explored by the host laboratory.

Keywords: Chronic Pain; voltage-gated potassium channels; dorsal root ganglia.

1. INTRODUCTION

1.1. Perception of Pain and Nociception

Pain is the most frequent cause of medical consultation, accounting for 25-50% of all consultations of General Practice. Of these consultations, 20% are motivated by chronic pain (Finnerup et al. 2007), which may affect 22% of the population that uses the primary health care (Lepine & Briley 2004). Pain is an unpleasant feeling of utter most importance for the body's defense system, as it provides a rapid warning to the nervous system to initiate a motor response to minimize potential physical harm. Pain is defined by the International Association for the Study of Pain (IASP) as "*an unpleasant sensory and emotional experience associated with actual or potential tissue damage, or described in terms of such damage*" (International Association for the Study of Pain). This setting recognizes pain as a subjective sensation, even in the absence of a demonstrable tissue injury, sustaining a well-known aphorism: "Pain is when the patient says it hurts" (McCaffery & Beebe 1989). Lack of the ability to experience pain as, for instance, in the rare congenital insensitivity to pain with anhidrosis (Axelrod & Hilz 2003) is very dangerous. This can cause very serious health problems such as self-mutilation, auto-amputation, and corneal scarring.

Nociception refers to the molecular mechanisms that underlie the detection of pain-producing stimuli by activation of specialized sensory receptors (nocipetors). Nociception is defined by IASP (International Association for the Study of Pain) as "*nerve noxious stimuli process of coding*", which are in turn defined as "*harmful stimuli or which threaten to damage the normal tissues*". These stimuli are responsible for the activation of *nociceptors*, defined by the same organization as receptors of "*high threshold, capable of transducing and encode noxious stimuli*." Thus, according to the IASP, nociceptive pain can be defined as an "*effective pain arising from a damage or damage of a threat, a non-nervous tissue, due to the activation of nociceptors*". Thus, stimuli perceived as painful are those likely to cause tissue damage. The nociceptive pain is usually transient, disappearing with tissue repair. In some conditions, excitation of pain fibers becomes greater as the pain stimulus continues, leading to a condition called hyperalgesia, which stands for an increased sensitivity to noxious stimuli (Hart 1988).

In short, *nociception* provides information about tissue damage, *pain* is the unpleasant emotional experience that usually accompanies nociception (Julius 2001).

1.1.1. NOXIOUS STIMULI, RECEPTORS AND PAIN PERCEPTION ASCENDING PATHWAY

Nearly a century ago, Sherrington proposed the existence of the nociceptor, a primary sensory neuron that is activated by stimuli capable of causing tissue damage and is able to provide information about that stimuli (Sherrington 1906). Nociceptors do not fire spontaneously at rest (Purves D, Augustine GJ, Fitzpatrick D 2001). Their electrical action potential is triggered by transduction, which occurs when a noxious stimulus of sufficient strength depolarizes the nociceptor membrane. The specific receptive properties of nociceptors are determined by their expression of transducing ion-channel receptors (Fein 2012). These ion channels are nonselective potassium or sodium channels gated by temperature, chemical stimuli, or mechanical shearing forces rather than by voltage. Activation of the channels by an appropriate stimulus leads to an inward current that depolarizes the receptor membrane (Julius & Basbaum 2001). If this depolarizing current is sufficient to activate voltage-gated sodium channels, further depolarization of the membrane will occur, and a burst of action potentials will be initiated. The duration and frequency of this burst are primarily determined by the duration and intensity of the noxious stimulus. Many, but not all, of these transducing receptors have been identified (Julius & Basbaum 2001).

Potentially damaging mechanical, thermal, and chemical stimuli, our noxious stimuli, are detected by nociceptors (found in different concentration the skin, on internal surfaces such as the periosteum, joint surfaces, and in some internal organs). Nociceptors are unspecialized free nerve endings that have their cell bodies outside the spinal column in the dorsal root ganglia (Purves D, Augustine GJ, Fitzpatrick D 2001). The dorsal root ganglia (DRG) is the segmental sensory ganglia of the spinal cord that contains the first-order neurons of the dorsal column and spinothalamic pathways (Julius & Basbaum 2001).

Chemical substances that modulate the transmission of painful stimuli are released into the extracellular tissue when tissue damage occurs. They activate the pain receptors by irritating nerve endings. These chemical mediators include histamine, substance P, bradykinin, acetylcholine, leukotrienes, and prostaglandins. These mediators can produce other reactions at the site of injury, such as vasoconstriction, vasodilatation, or altered capillary permeability. For example, prostaglandins induce inflammation and potentiate

other inflammatory mediators (Matsuka et al. 2001; Waxman & Zamponi 2014; Helms & Barone 2008).

In this context, pain has a protective role as it motivates a response to damaging situations to protect a damaged body part while it heals and to avoid similar experiences in the future through the formation of memory (Holden & Winlow 1984). In this context, specificity is not imperative (Schaible 2007). Most high-threshold receptors respond to a variety of thermal, chemical and mechanical stimuli and are defined as polymodal nociceptors.

Recently, cell ablation studies using the Cre-loxP system (Sauer 1987) have demonstrated that distinct sensory subpopulations underlie distinct pain modalities, distinguishing mechanical and thermal pain (Abrahamsen et al. 2008; Mishra et al. 2010).

Nociceptors can be distinguished according to their differential expression of channels that confer sensitivity to heat (TRPV1), cold (TRPM8), acidic milieu (ASICs), and a host of chemical irritants (TRPA1), see Figure 1 below (Julius & Basbaum 2001).

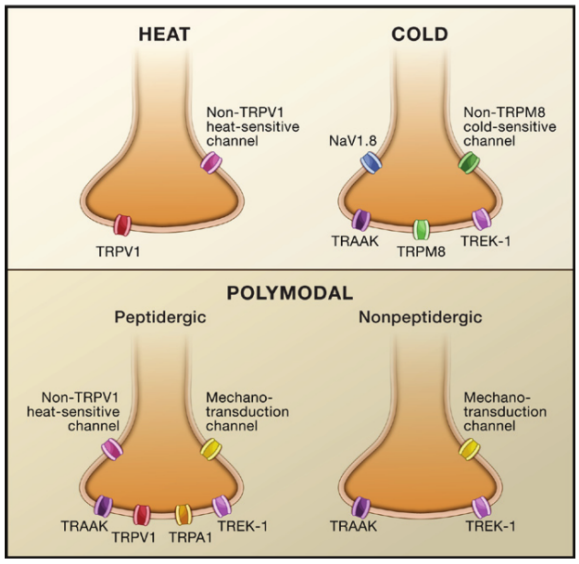

Figure 1 Nociceptor Diversity There are a variety of nociceptor subtypes that express unique repertoires of transduction molecules and detect one or more stimulus modalities. For example, heat-sensitive afferents express TRPV1 and possibly other, as yet unidentified heat sensors; the majority of cold-sensitive afferents express TRPM8, whereas a small subset likely express an unidentified cold sensor. Polymodal nociceptors also express chemoreceptors (e.g. TRPA1) and one or more as yet unidentified mechanotransduction channels. These fibers also express a host of sodium channels (such as NaV 1.8 and 1.9) and potassium channels (such as TRAAK and TREK-1) that modulate nociceptor excitability and/or contribute to action potential propagation.

Nociceptors have a certain threshold of activation (minimum intensity of stimulation) they require to transduce a given signal. If the stimuli is strong enough to reach the threshold, the resulting depolarization activates voltage-gated calcium (Ca^{2+}) and sodium (Na^{+}) channels present at the terminals of nerve fibers to initiate an action potential. This is conducted along the axon of the neuron into the spinal cord, following an afferent pathway from periphery into the central nervous system, as represented in Figure 2. (Purves D, Augustine GJ, Fitzpatrick D 2001). Voltage-gated sodium and potassium channels (Nav

and Kv, respectively) are critical to the generation of these action potentials that convey nociceptor signals to synapses in the dorsal horn.

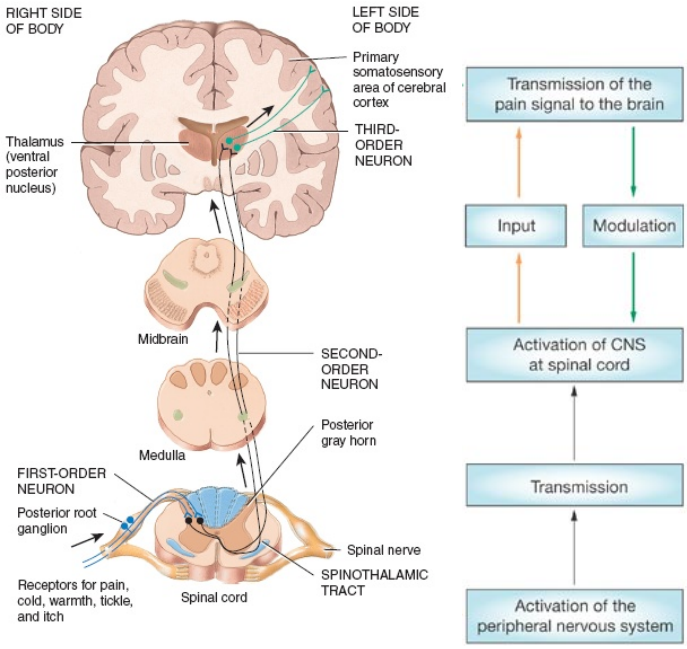

Figure 2 The ascending spinothalamic pathway. The anterolateral pathway conveys nerve impulses for pain, cold, warmth, itch, and tickle from the limbs, trunk, neck, and posterior head to the cerebral cortex.

1.1.2. RAPID SIGNAL TRANSMISSION

Neurons are the cellular units of the nervous system which are highly differentiated while interconnected and bioelectrically driven (Margrie & Urban 2007). There are mainly three types of neurons: afferent, interneurons and efferent. The first are responsive neurons that transduce external stimuli. The interneurons transmit the signal from the afferent neurons to the central nervous system, and are the link between afferent and efferent neurons. Finally, there are efferent neurons whose function is to transmit the signal from the central nervous system to the effector organ (Ludwig & Pittman 2003).

Communication between neurons is largely aided by the existence of *clusters* – nerve cords – of axons linked together. This way, the cells are in high proximity of each other, which enables faster and efficient communication: this is denominated *centralization* (Margrie & Urban 2007). In this context, DRG are clusters of cell bodies of neurons that give rise to the first-order neurons that innervate regions of the body, which aids fast communication.

The nerve fibers within a nerve include both afferent nerves and efferent (motor and autonomic) nerves (von Kitzing et al. 1994). The afferent nerve fibers innervate and communicate with the dorsal side of the spinal cord i.e., the dorsal horn and thus responsible for conducting information into the spinal cord (ascending pathway into the brain – see Figure 1); the efferent nerve fibers innervate and communicate with the ventral side of the spinal cord and are responsible for the descending pathway of the brain and so conduct the information out of the spinal cord (Nashmi & Fehlings 2001).

The speed at which an individual nerve fiber conducts action potentials is related to the diameter of the fiber and on the existence of a myelin sheath (Campbell & Meyer 2006). The myelin sheath has a great amount of cytoplasm compacted which accelerates the propagation of the signal through saltatory conduction, without the enlargement of the axon. In the areas of the axon unmyelinated, the membrane is relatively thin, so the attraction force between cations outside the membrane and the anions inside the membrane is very high, high enough to overpower the force of repulsion between same charge ions in each side of the membrane (Kendall 1999). By augmenting the membrane thickness through the myelin sheath there is a decrease in the compaction of charges in the myelinated areas which facilitates the membrane depolarization and the signal propagation (Campbell & LaMotte 1983).

These fibers can be categorized into three main groups as seen below on Figure 3a: Aβ-, Aδ- and C-fibers (Fein 2012). Cell bodies with the largest diameters give rise to myelinated, rapidly conducting Aβ-primary sensory fibers. Most, but not all (Djouhri et al. 1998), Aβ fibers detect innocuous stimuli applied to skin, muscle and joints and thus do not contribute to pain – prioperception (see Figure 3) (Julius 2001). The other two, the small- and medium-diameter fibers and thus cell bodies, are the fibers that contribute to nociception (Fein 2012; Djouhri & Lawson 2004). There are many differences between the two types of fibers, but the one that stands out the most is the presence/absence of a myelin sheath. As stated before, the myelin sheath is the main protagonist in action potential conduction velocity. C-fibers are slowly conducting fibers since they are unmyelinated and therefore responsible for a delayed, more diffuse, dull pain evoked by noxious stimuli while Aδ-fibers are thinly myelinated, relatively more rapidly conducting, and mediates a rapid, acute, sharp pain (Figure 3) (Djouhri & Lawson 2004).

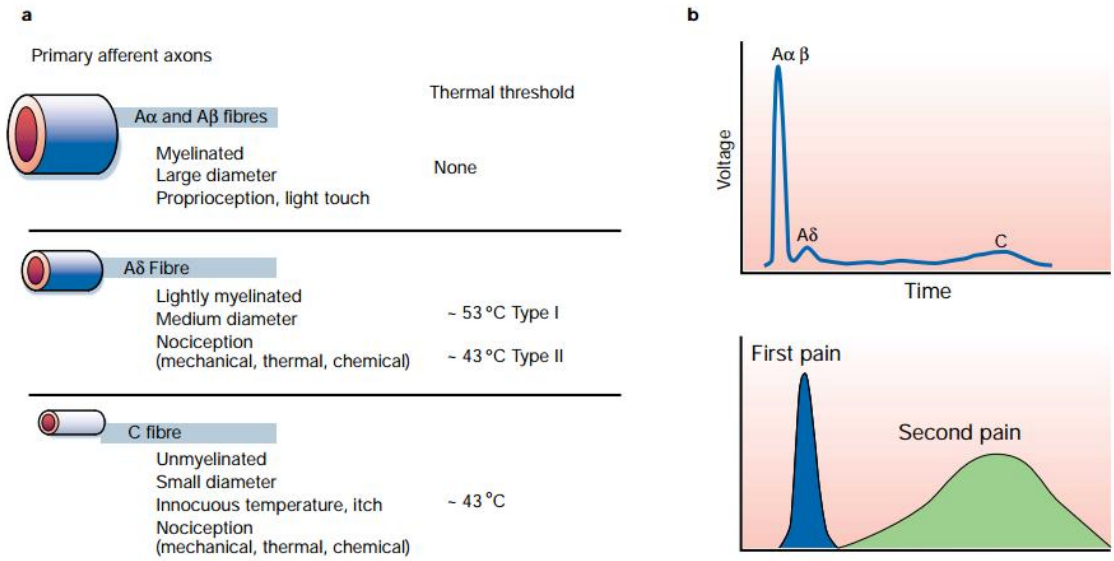

Figure 3 Different nociceptive fibers and characteristics. Different nociceptors detect different types of pain. **a.** Peripheral nerves include medium-diameter (Aδ) and large-diameter (Aβ) myelinated afferent fibers, as well as small-diameter unmyelinated afferent fibers (C). **b.** Most nociceptors are either Aδ or C fibers, and their different conduction velocities account for the first (fast) and second (slow) pain responses to injury. Adapted from Fields, 1987.

1.1.3. ASCENDING SPINOTHALAMIC PAIN PATHWAY

The signal travels from the free nerve endings to the cell bodies of the nociceptors that are located in the dorsal root ganglia (DRG) for the body and in the trigeminal ganglion for the face (Basbaum et al. 2009). Noxious signals originated from the periphery are transmitted by C-fibers and Aδ-fibers to the secondary neurons in the dorsal horn of the spinal cord. C-fibers project to the nociceptive upper laminae of the dorsal horn, whilst the Aδ-fibers projects to the deeper laminaeof the dorsal horn (Dib-Hajj et al., 2012).

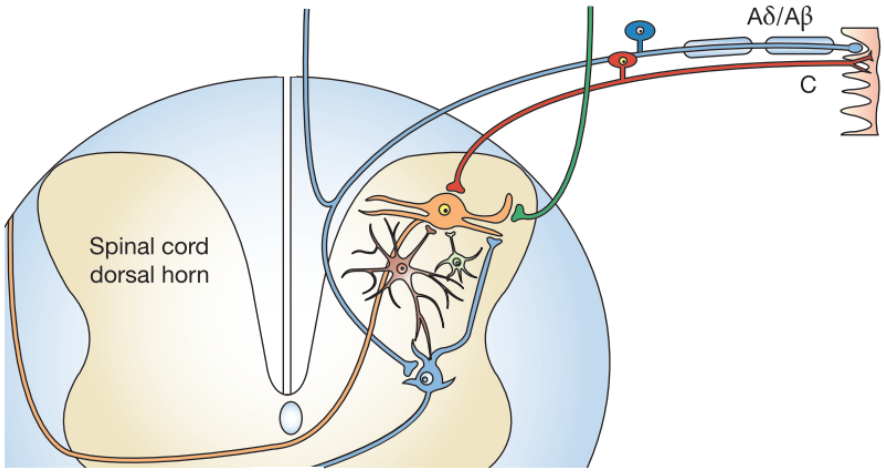

Figure 4 Primary afferent pathways and their connections in the spinal cord dorsal horn. Nociceptive C-fibers (red) terminate at spinothalamic projection neurons in upper laminae (orange neuron), whereas myelinated A-fibers (blue) project to deeper laminae. Adapted from (Baron 2006).

The first-order neurons from C fibers synapse with the secondary sensory neurons at the dorsal horn of the spinal cord, releasing neurotransmitters such as glutamate or substance P (Basbaum et al. 2009). As described by Purves D, Augustine GJ, Fitzpatrick D, 2001, once within the dorsal horn, the C-fibers send branches to innervate neurons in Rexed's lamina I and lamina II, while the Aδ-fibers terminates in the lamina II and V (Dib-Hajj et al. 2012; Fukuoka & Noguchi 2011). Finally, the large mechanosensor fibers sprout to the laminae III and V of the dorsal horn (Belkouch et al. 2014). The information is then transmitted to second-order neurons that cross over the spinal cord and ascend all the way to the brainstem and thalamus in the anterolateral quadrant of the contralateral half of the spinal cord (see Figure 2**Error! Reference source not found.**). There, the second-order neuron then synapses with a third-order neuron in the medial and ventrobasal nuclei of the thalamus by releasing neurotransmitters. This third-order neuron synapes with the somatosensory cortex of the brain which locates the injured area of the body and

coordinates appropriate pain perception (see Figure 2) (Nicholls, J. G., Martin, A. R., & Wallace 1992).

1.2. When Pain Becomes a Dysfunction

1.2.1. CHRONIC PAIN SYNDROME

As aforementioned, pain has a protective and informative role in people's lives. This kind of pain terminates once the noxious stimuli is removed and the body has healed. However, pain may outlast its practicality as a warning sign and become chronic (Raj et al. 2007).

Pain is defined as chronic rather than acute not only on the basis of its duration but also on the basis of the body's inability to restore physiologic function to homeostatic levels. The intensity of chronic pain has little relation to initial tissue damage or subsequent pathology as psychological and social factors seem to have great influence (Kendall 1999).

Chronic pain is a heterogeneous disease in terms of its etiology, mechanisms and temporal properties (Russo MD & Brose MD 1998; Azevedo et al. 2012). The three main etiologies for chronic pain are presented in the following sections. Understanding the cellular mechanisms underlying chronic pain is a critical step in the development of new therapies.

Abnormally amplified signals in the central nervous system due to wind up in central sensitization (which is an increased sensitivity of spinal neurons) cause primary and secondary hyperalgesia (an exaggerated sensation to a painful stimuli at the site of the injury and surroundings, respectively) and allodynia (perception of pain in response to a non-painful stimuli) (Tsantoulas & McMahon 2014; Russo MD & Brose MD 1998; Campbell & Meyer 2006). Symptoms usually include spontaneous paresthesia (abnormal sensation), such as numbness, pain with movement, sensitivity of a partly denervated body part and burning, tingling sensation (Milton 2013).

1.2.2. CELLULAR MECHANISMS OF NEUROPATHIC PAIN

Neuropathic pain syndromes are chronic pain disorders caused as a direct consequence of a lesion or by disease of the parts of the nervous system that normally signal pain (Baron 2006). When a lesion occurs on the nerves, the expression of Nav channels is increased and Kv channels is decreased in the affected fibers and the myelinated damaged fibers undergo a Wallerian degeneration. During this process, they release nerve-growth factor (NFG) which contacts with the intact fibers from the neighbouring axon. They increase the expression of Na^+ channels, TRPV1 channels and adrenoreceptors and the decrease of K^+ channels, therefore increasing the sensitivity of those uninjured fibers (Baron 2006).

1.2.3. CELLULAR MECHANISMS OF INFLAMMATORY PAIN

Pain is the primary reason patients with inflammatory arthritis seek rheumatologic care. Among rheumatoid arthritis patients, 68-88% rate pain as one of their top three priorities (Turk et al. 2004). Local inflammatory pain may appear in the absence of nerve trauma, as in the patients with low back pain or postherpetic neuralgia, which is a complication of shingles, caused by the chickenpox virus (Abrahamsen et al. 2008).

Inflammatory pain results from the sensitization and activation of peripheral nociceptors by inflammatory mediators that accumulate in damaged tissue. The action of inflammatory mediators upon primary sensory afferents causes these neurons to have increased excitability, contributing to pain and hypersensitivity, also featuring hyperalgesia, allodynia and spontaneous pain (Abrahamsen 2014).

1.2.4. CELLULAR MECHANISMS OF PAINFUL DIABETIC NEUROPATHY

Peripheral diabetic neuropathy is characterized by diffuse or focal damage of somatic or autonomic peripheral nerve fibers, resulting from diabetes mellitus (Iyer & Tanenberg 2013). One of the most prominent features of diabetic neuropathy is the development of spontaneous pain, typically in the extremities, presenting as allodynia and hyperalgesia (Tesfaye & Kempler 2005), as it results from the atrophy and loss of myelinated and non-myelinated fibers accompanied by Wallerian degeneration (Iyer & Tanenberg 2013).

1.3. Neuroexcitability

1.3.1. RESTING MEMBRANE POTENTIAL

Action potentials are generated across the membrane of the neuron, which then sends an electrical signal along the membrane of the axon (Hille 2001). When the membrane is at rest, it has a much higher concentration of Na^+ on the extracellular side in comparison to the intracellular side and vice-versa for K^+ concentration (Cooper et al. 1998). Regarding the electrochemical gradient, the membrane of the neuron is much more permeable to K^+ than to Na^+. But the membrane is also richer in channels that facilitate the diffusion of K^+ than Na^+ and therefore, more K^+ will leave the cell than Na^+ will enter (Armstrong & Hille 1998; Hille 2001; Hodgkin & Huxley 1952).

Considering only K^+, as the ions leave the cell, the positive charges decrease on the inner side of the membrane and increase on the outer side. As positive charge builds on the extracellular side, the electric force begins to drive the K^+ back inside. Equilibrium is reached when the electric force is equal to the force of the concentration gradient.

1.3.2. VOLTAGE-GATED ION CHANNELS

As pointed out by Hodgkin & Huxley, mobile charge in the membrane that moves in response to voltage changes is the only possible way of having voltage dependence on the opening and closing of the gate (Hodgkin & Huxley 1952).

The channel current is important as a measurement of the speed of movement of ions through the channel. The current depends not only on the properties of the channel as well as the transmembrane potential (Margrie & Urban 2007). The conductance of a channel depends on two factors: (1) the ease with which ions can pass through the channel – permeability; (2) the concentration of ions in the channel region. One can measure the membrane current through its channels conductance and the voltage applied (Southan & Robertson 2000).

1.3.3. WHY K^+ CHANNELS?

Electrical signals result from temporary local changes that drive membrane potential away from its resting value and are propagated throughout a neuron or nervous fiber. Ion channels mediate those alterations (Bezanilla 2005; Julius & Basbaum 2001; Margrie & Urban 2007). They are divided into families depending on structure and function. For this dissertation, the main focus will be on voltage-gated potassium channels that respond to changes of voltage across membrane (Kv channels).

Membrane proteins account for about 30% of the total proteome of an organism, with about half of this number being carrier proteins and ion channels. K^+ channels represent the most diverse and widespread class of membrane proteins (Frank et al. 2005). Of those, Kv channels form the most diverse group, represented by 12 families (Kv1-Kv12) (Gutman et al. 2005; Bosma & Hille 1992).

Kv channels have several important characteristics as they are highly restricted locations in axons, show diverse mechanisms of clustering, and, importantly, they contribute to neuronal excitability through setting the resting membrane potential and spike interval (Misonou 2010; Nashmi & Fehlings 2001). In excitable cells, Kv channels are involved in the stabilization of the membrane potential, since they converge the resting membrane potential to the K^+ equilibrium potential, lowering it, and therefore keeping it away from the action potential firing threshold (Bosma & Hille 1992). Hence, they are critical to neuroexcitability. Not only they establish the resting potential but also keep the depolarization in the action potential short, are involved in shortening periods of high activity, keep a time separation between repetitive spikes and tend to diminish the excitatory inputs efficacy in the cell (Bosma & Hille 1992).

These multisubunit integral proteins mediate K^+ fluxes depending on their level of expression, conduction properties, activation, deactivation and inactivation characteristics, and the electrochemical gradient of ions across the cell membrane (Yellen 2002; Miller 2000). For instance, mutations in the genes of Kv channels can lead to several severe hereditary disorders (Camacho 2006; Wang et al. 1996), and importantly to this work, they are involved in the development of the pain syndrome (Beekwilder et al. 2003).

1.3.4. KV CHANNELS IN DRG NEURONS

As aforementioned, K^+ channels are a family of ion channels that govern the intrinsic electrical properties of neurons (Lujan 2010). Molecular cloning has revealed over 100 genes encoding the pore-forming α-subunits of K^+ channels in mammals, making them the most diverse subset of ion channels. Further multiplicity of the K^+ channel family is generated through alternative splicing. The precise location of K^+ channels along the dendro-somato-axonic surface of the neurons is a crucial factor in determining its functional impact (Doyle et al. 1998; Calvo et al. 2016).

Sensory neurons express multiple types of Kv channels, including members of the Kv1, Kv2, Kv3, Kv4, Kv7 and Kv9 families, with expression patterns depending on neuronal subtype. Immunochemical studies suggest that numerous Kv channels in the Kv1 and Kv2 family are expressed in DRG neurons (Kuniko Ishikawa et al. 1999). This is in agreement with the presence of RNA transcripts encoding for Kv1, Kv2, and, in addition, Kv4 subunits in the DRG. Among the Kv1 channel family, the most abundantly expressed channels in DRG neurons are Kv1.1, Kv1.2 and Kv1.4 (Yang et al. 2004; Rasband et al. 2001; Kim, Choi, Rim, Cho, et al. 2002; Vydyanathan et al. 2005). Of these, Kv1.4 appears to be the most abundant Kv isoform in DRG neurons as most small diameter DRG Kv1.4-positive neurons do not detectably express other Kv1 subunits (Wells et al. 2007).

Corroborating with Kv1.4 high proportion to other isoforms, small-diameter DRG neurons predominantly express an A-type K^+ current whose properties correspond well with those expected for homotetrameric Kv1.4 channels (Sigworth 1994).

Not disregarding the presence of other Kv1 isoforms, Kv1 family channels are important determinants of neuronal excitability (Doyle et al. 1998). For instance Kv1.2 lowers excitability at the level of the sensory neuron cell body (Rasband et al. 2001; Everill et al. 2014) and Kv1.1 decreases mechanosensitivity (the mechanical sensitivity threshold gets higher) at the terminals of C-mechanonociceptor (Hao et al. 2013).

1.3.5. INVOLVEMENT OF DRG KV CHANNELS IN CHRONIC PAIN

Following nerve injury, DRG neurons can display aberrant firing properties or cross-excitation by neighboring neurons (Frank et al. 2005), producing inappropriate impulse activity that may underlie abnormal sensations.

The contribution of K^+ channels in pain signalling has been undervalued over the years, as research has been mainly focused on studying Na^+ and Ca^{2+} channels. However, emerging data has highlighted that nerve injury or inflammation alters K^+ channel activity in neurons of the pain pathway, having a prominent role on DRG hyperexcitability, thus starting to reveal its potential as a novel therapeutic target (Tsantoulas & McMahon 2014; Cao et al. 2011; Rasband et al. 2001; Wulff & Castle 2009).

Multiple studies have demonstrated downregulation of expression of K^+ channels in animal models of pain. For instance, a downregulation of Kv1.2 channels in DRG neurons in response to nerve injury has been reported (Fan et al. 2014) and is linked to myeloid zinc finger protein 1 (MZFP1) mediated expression of an endogenous antisense-like RNA (see Figure 5). As a result, excitability of afferent fibers is enhanced, leading to neuropathic-like pain behavior that can be attenuated by delivery of Kv1.2 sense fragments.

Chronic bladder inflammation increases the excitability of C fiber bladder afferent neurons through

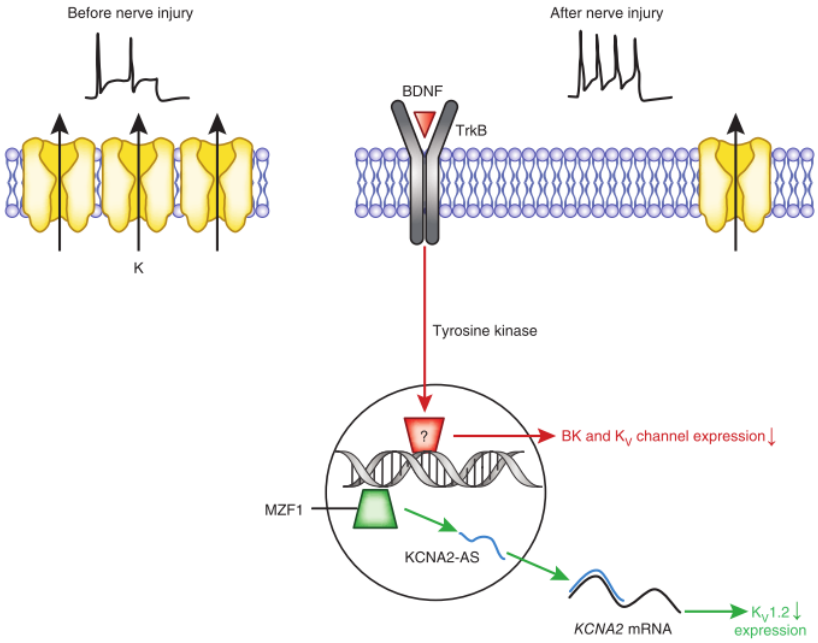

Figure 5 Examples of mechanisms of nerve injury – induced inhibition of K^+ channel expression. Under normal physiological circumstances, the activities of Kv channels limits the firing of afferent fibers (top left). In response to nerve injury BDNF activates TrkB receptors, which then regulate the expression of Kv channels at the transcriptional level, leading to reduced KV1.2 protein expression. The reduction of potassium channel expression leads to increased firing of injured neurons (top right). Reproduced from Waxman & Zamponi 2014.

suppression of Kv1.4 channels (Yoshimura & Groat 1999), which suggests these A-type

channels are a major determinant of C fiber excitability. This is of particular importance when considering pharmacological treatment of pain. An alternative to reducing nociceptor excitability through blockade of action potential depolarization may lie in enhancing or prolonging activity of Kv1.4. This might be accomplished by interfering with the ball-and-chain N-type inactivation (explained below at section 1.3.8) that among Kv1 subunits is unique to Kv1.4 (Wells et al. 2007).

It has also been shown that Kv1.3 is present in DRG nociceptive neurons, which is a channel partly responsible for the slowly inactivating K^+ current. This channels has been shown to be downregulated in whole lysates of DRG (Yang et al. 2004) in sciatic nerve transection chronic pain model. Also, Abdulla and Smith (2001) observed a significant decrease in steady-state mRNA level of Kv1.3 (about 50%) in all types of DRG neurons in axotomized rats that led to increased neuroexcitability. Although this channel appears to be downregulated in chronic pain models, the slowly inactivating current does not appear to be as affected as the A-type current due to their contributing channel proportion in small-diameter DRG neurons (Fukuoka et al. 2012; K Ishikawa et al. 1999)

Altogether, these various studies associate Kv channels as modulators of inflammatory and neuropathic pain signaling in afferent neurons. Specifically, they suggest a reduction of both slowly inactivating and A-type K^+ currents through the downregulation of Kv channels.

1.3.6. KV CHANNELS CONFORMATIONS

All Kv channels share a high level of similarity. Each Kv channel gene encodes one α-subunit and functionality requires four, hence Kv channels present a homotetrameric structure (with all α-subunit being identical) (Grizel et al. 2014). The transmembrane domain of the Kv channel α-subunit consists of six helices: S1 – S6. These helices form two structurally and functionally different parts of the tetrameric channel (Long et al. 2005):

1) K^+-conducting domain (pore domain) – helices S5–S6 located in the center;

2) Voltage-sensing domain – helices S1–S4 located on the channel periphery.

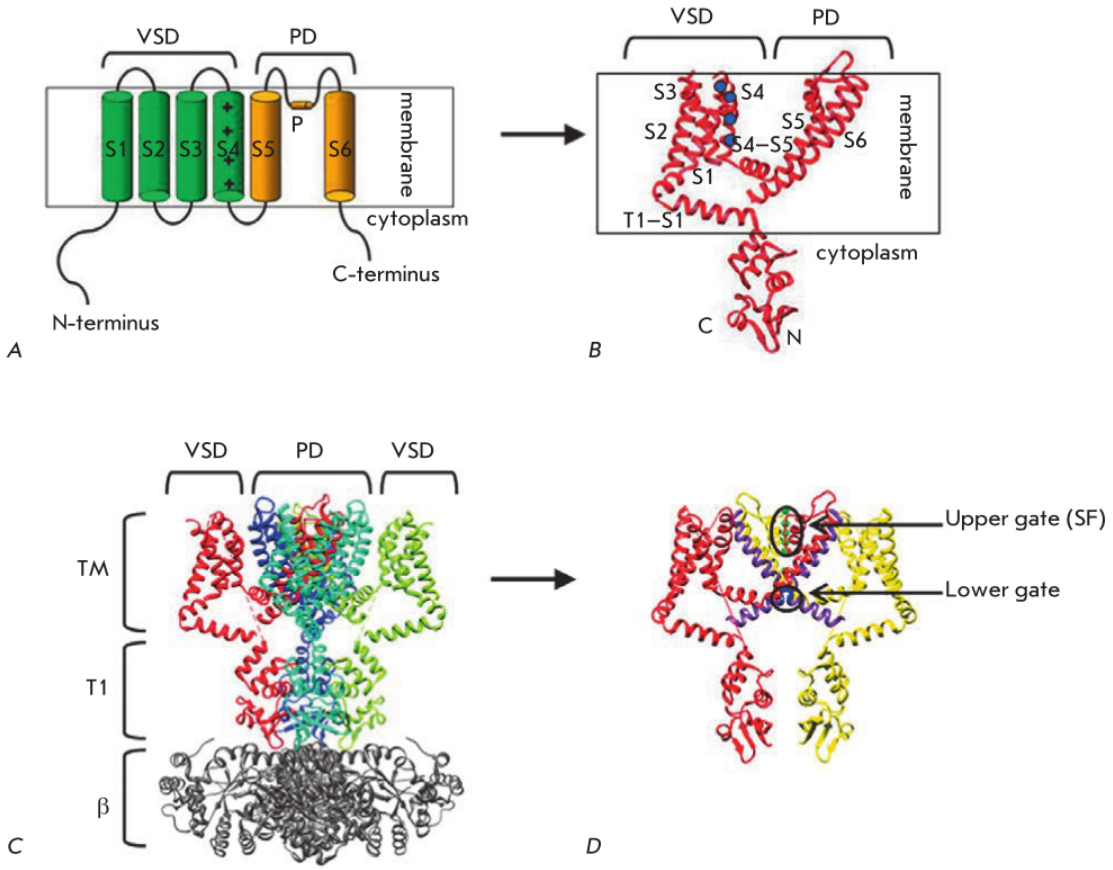

Figure 6 Secondary, tertiary and quaternary structure of Kv channels. A. Scheme of a single α-subunit of a Kv channel: Transmembrane segments S1–S6 and pore-forming P-region are marked. Charged Arg of the membrane voltage sensor S4 are marked with "+" signs. **B.** Crystal structure of a single α-subunit: S1–S6 segments, cytoplasmic domain T1, linker connecting the transmembrane portion with the T1 domain (T1–S1), as well as N- and C-termini are marked. Charged Arg residues of the membrane voltage sensor S4 are indicated by blue circles. **C.** Crystal structure of the Kv1.2 channel in a complex with the β-subunit (grey). **D.** Upper and Lower gates. Only two opposite subunits of Kvα are shown for clarity reasons. Figure replicated from (Grizel et al. 2014)

The pore domain includes a channel gate and a selective filter that only allows K^+ to enter through the channel. It is constituted by carbonyl groups which are spaced to interact with unsolvated K^+. This way the passage of a Na^+ through the channel is energetically unfavorable because the Na^+ is too small for optimal interaction with the carbonyl groups.

The channel gate is formed by crossing C-termini of the S6 helices that block passage of ions when the channel is closed (Doyle et al. 1998; Choe 2002).

It is known that the voltage sensing domain and the pore domain are covalently bound by the S4–S5 linker, which is a helix connected to the C-terminus of S6 helix and the next subunit (Choe 2002). This is a highly conserved region, which plays an important role in opening/closing the channel gates due to its flexibility. (Grizel et al. 2014).

Kv channels have two gates (Figure 6.D):

1) Lower gate formed by crossing the S6 helices on the intracellular side: this is the main activation gate controlled by external stimuli, such as the membrane potential;
2) Upper (inactivation) gate formed by the P-region of the selectivity filter on the extracellular side.

The cytoplasmic part does not contain highly conserved regions and is different for Kv channels from different families (Pischalnikova & Sokolova 2009). β subunits (or auxiliary proteins), with distinct sequences, also often interact with the principal subunits complex, usually altering their electrophysiological or biophysical properties, expression levels or expression patterns (Coetzee et al. 1999).

1.3.7. ACTIVATION OF KV CHANNELS

Kv channels (and voltage-gated channels in general) exist typically in three different conformations that are inter-commutable: the activated state, associated with an open conformation – both gates open; inactivated state, associated with a non-conducting conformation – only one gate open and the other closed; and a quiescent state, associated with a closed conformation – both gates closed (Armstrong 2003)

The channel does not conduct the ions in the quiescent state. Depolarization of the membrane results in positive charge of its intracellular part, causing conformational rearrangements of Kv channels and making an open conformation energetically favorable, i.e., activation (Sigworth 1994; Coetzee et al. 1999; Grizel et al. 2014). In case the membrane remains depolarized, the majority of Kv channels switch to the inactivated non-conducting state.

The selectivity filter is in near proximity to the S4 transmembrane domain,

which is the voltage sensor. Its cationic properties are due to its high arginine and lysine amino acids residue constitution. At rest, this positively charged domain is attracted to the inner residues of S2 and S3. When a depolarization occurs, the intracellular side of the membrane becomes less negative. As the S4 is positively charged, during depolarization this domain is electrostatically repelled upward, into the membrane, away from the cytoplasm. This allows ion conductance through the channel (Southan & Robertson 2000; Miller 2000). The exact mechanistic behind the activation of Kv channels is yet to be understood (Horn 2005; Grizel et al. 2014).

1.3.8. INACTIVATION OF KV CHANNELS

There were described two inactivation mechanisms for Kv channels during prolonged depolarization:

1. *Fast N-type inactivation*: The inactive state is mainly achieved through fast inactivation, by which a channel transitions rapidly from an open to an inactivated state. The model proposes that the inactive state, which is stable and non-conducting, is caused by the physical blockage of the pore. The blockage is mediated by an inactivation peptide positively charged folded into a globule and attached by a linker to the N-terminus. As the S4 is repelled into an upward position, the globule is dragged into the open pore of the channel and blocks ion traffic (Nicholls, J. G., Martin, A. R., & Wallace 1992). Importantly, Kv1.4 is the only Kv1 isoform that has this kind of inactivation.

2. *Slow C-type inactivation*: the selectivity filter acts as the second gate, as the C-terminus often carries motifs for channel modulation other than voltage, such as phosphorylation and Ca^{2+} binding (Robbins 2001). In cases of prolonged depolarization, the pore closes, preventing the entry of ions (Leung 2012). The channels completely return to the closed conformation after the inactivation when the potential drops to the resting potential level. The Kv1.3 channel shows a slow C-type inactivation and recovery (Southan & Robertson 2000).

1.3.9. KV CURRENTS IN DRG

Early electrophysiological characterization of DRG neurons revealed two types of voltage-gated K^+ currents: transient (inactivating) A-type current (I_{fast}) and a slowly

inactivating (I_{slow}) (Mathie et al. 1998; Kostyuk et al. 1981; Yang et al. 2004). Within both types of currents further biophysically and/or pharmacologically distinct components can be identified and these differ between the sensory neuron types. Criteria for their identification include rapid activation and inactivation, dependence on the holding potential, and sensitivity to both 4-AP and DTx (Wu & Barish 1992). For instance, I_{fast} currents can be dissected from the sustained current using two different prepulse voltages with identical stimulation pulse protocols (Everill et al. 1998).

Figure 7 shows current families found in all DRG neurons from L4-L5 ganglia recorded at voltages between −40 and +50 mV after a 500 ms conditioning prepulse to −120 mV or to −40 mV.

- Figure 7A1 demonstrates the main composition of currents occurring in ~58% of cells examined (Everill et al. 1998). Subtraction of responses (Figure 7A3) revealed fast and slow activating and inactivating components that were sensitive to the prepulse variation.

- Figure 7B shows that in some of the neurons the K^+ current components (~24%, Everill et al. 1998), I_{fast} and I_{slow}, were clearly defined after subtraction.

- Figure 7C3 displays the slower inactivating component. Cells lacking I_{fast}, but showing the slower inactivating component were seen in ~12% of the cells examined (Everill et al. 1998).

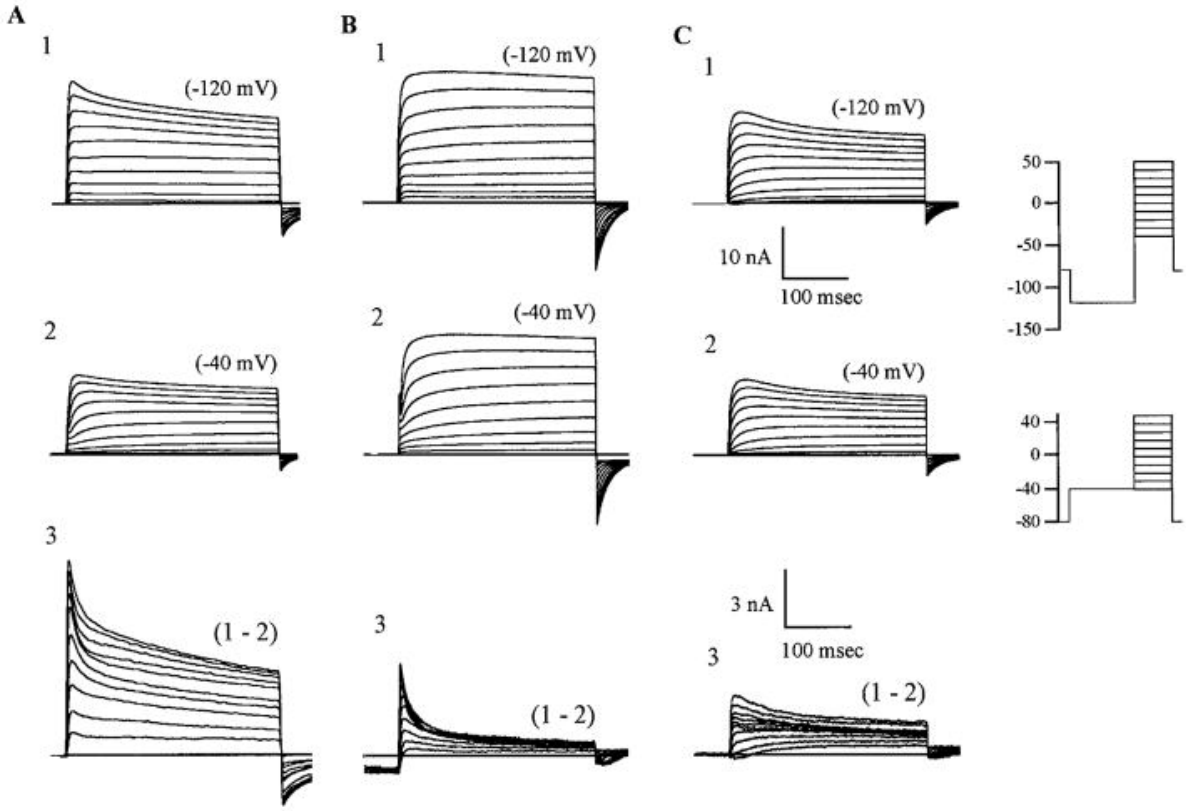

Figure 7 Voltage-dependent potassium currents of DRG neurons. Recordings from 3 categories can be seen in A1, B1, and C1 recorded after the −120-mV prepulse protocol; A2, B2, and C2 were initiated via the −40-mV prepulse protocol. A: typical type of traces (of this shape and amplitude) that were recorded in the majority of experiments. This cell type manifested ≥3 distinct components of current. B1–B2: this cell type has a large amount of fast inactivating component in its complement of currents. C1–C2: cell type that lacks the fast inactivating component but has a slower inactivating voltage-activated component sensitive to the conditioning potential. Lower scale bars relate to subtractions only (subtractions are enlarged for clarity of comparison). These are typical traces taken from the mean of each group. Reproduced from Everill et al. 1998.

Functional investigations pointed out that I_{fast} is typically involved in setting the interspike interval (Hille 2001), while I_{slow} is essential for fast repolarization of action potentials and consequently contributes to repetitive firing pattern (Armstrong 2003).

1.4. Animal Pain Models

Rodent behavioural models are important tools for expanding the understanding of the physiology underlying nociception and pain (Mogil et al. 2010). Rat models result in nociceptive sensitization similar to the key components of those experienced in humans (Barrett 2015). The use of rodents to study chronic pain is also adequate because drugs that shown some efficacy in chronic pain patients have also demonstrated activity in animal models of pain (Li et al. 2015).

The rat behaviour in response to noxious stimuli can be consistently and objectively scored through different tests. However, the most reliable and commonly scored behaviours are simple reflexes or innate responses (such as paw withdraw, linking the sensitized zone, tail flick) (Mogil et al. 2010).

1.4.1. NEUROPATHIC PAIN: *CHRONIC CONSTRICTION INJURY (CCI)*

Neuropathic pain models rely on cutting, stretching or compressing the nerve and therefore, rely on a surgical approach (Mogil 2009). Following traumatic nerve injury spontaneous activity develops initially in myelinated and subsequently in unmyelinated sensory axons (Kajander et al. 1996; Austin et al. 2012). The onset of this spontaneous activity is associated with the emergence of pain-related sensory changes in animal models (Nashmi & Fehlings 2001).

One of the most usual neuropathic pain model used in rodent is the chronic constriction injury (CCI) in which the sciatic nerve is constricted with four loose ligations. The resulting constriction does not stop the blood flow and produces an inflammation, leading to the physiological changes inhered to chronic neuropathic pain in the DRGs located in the 4^{th}, 5^{th} and 6^{th} lumbar vertebrae (L4-L6) (Austin et al. 2012).

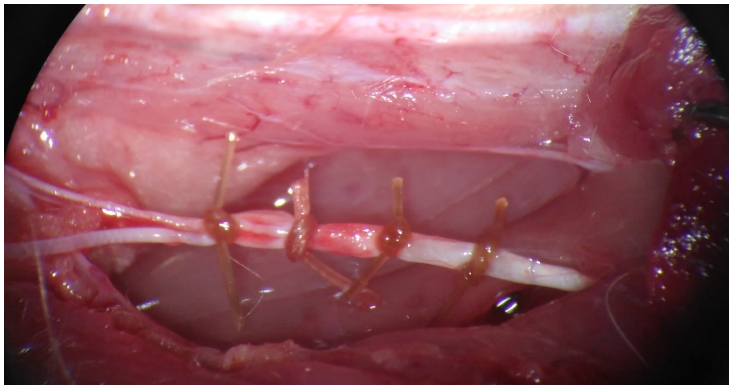

Figure 8 Photograph of the 4 loose ligations on mid-thigh sciatic nerve of a 65 days old female Wistar rat.

One limitation of this model is the degree of variation amongst the rats subjected to CCI, due to variability in the tightness of the constrictions produced by tying knots with the sutures. This can be partially overcome by having an experienced researcher performing the surgery in a consistent way. Furthermore, the type of suture material used for ligating the nerve can also contribute to variability (Attal et al. 1990).

1.4.2. INFLAMMATORY PAIN: *COMPLETE FREUND'S ADJUVANT (CFA)*

Complete Freund's Adjuvant (CFA) is a solution of antigen emulsified in mineral oil and consists of inactivated and dried mycobacteria. The CFA injection is a simple procedure which reproducibly induces inflammation, as shown in previous studies (Spears et al. 2005; Guan et al. 2005). However, single-dose CFA injections in previous work were primarily associated with transient inflammatory changes in the temporomandibular joint (Ren & Dubner 1999).

CFA is effective in stimulating cell-mediated immunity and leads to potentiation of T helper cells, which culminates in the production of certain immunoglobulins and effector T cells (Koo et al. 2013) therefore leading to inflammation and pain. The pain information is processed by the L3, L4 and L5 DRGs.

1.4.3. NEUROPATHIC PAIN: *PAINFUL DIABETIC NEUROPATHY (PDN)*

In order to induce Painful Diabetic Neuropathy (PDN), streptozotocin (STZ) has been largely used as an experimental paradigm for its great stability and relative lack of extrapancreatic toxicity (Sik Nam et al. 2014). STZ indirectly activates an apoptotic program that destroys pancreatic β-cells and all the cells expressing the GLUT2 transporter (Wattiez et al. 2012), leading to diabetes mellitus type I. Diabetes can lead to both mechanical hyperalgesia and hypoalgesia (Heng et al. 2015).

1.4.4. HOW TO EVALUATE PAIN IN ANIMALS

The area tested is the mid-plantar surface of the hind paw (Figure 9), which falls within the sciatic nerve distribution. Mechanical withdrawal threshold is assessed by mechanically stimulating both injured and uninjured hind paws using an electronic dynamic plantar von Frey aesthesiometer or manual von Frey filaments (Austin et al. 2012).

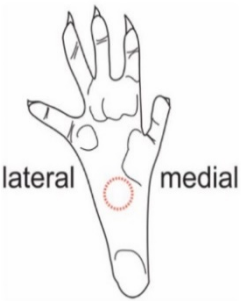

Figure 9 Diagram of the plantar surface of the hind paw.

The mechanical withdrawal threshold is the maximum pressure applied (in grams) that elicits paw withdrawal. This quantifiable measurement allows direct comparisons of paw sensitivity to mechanical stimuli across different treatment options, and between different strains of rats.

It should be noted that other behavioural assays, such as the pin prick test, cold allodynia, vertical activity and open field exploration are also used for testing pain hypersensitivity.

2. GOALS

The neurons of the dorsal root ganglia (DRG), are the main experimental model in studies of the physiology of pain. DRG neurons, and in particular the small-diameter DRG neurons, have great interest to the pharmaceutical industry dedicated to the research and development of new analgesics since its activity is involved in the processing of pain perception, which is exacerbated in chronic pain situations. A most promising therapeutic approach for chronic pain is to reduce neuronal hyperexcitability that occurs in this condition, which can be done by altering the current of the main ion channels that modulate the electrical activity of DRG neurons. The knowledge about the voltage-gated K^+ (Kv) channels is essential since these channels control excitability and some of them are already seen as molecular targets for the development of new analgesics. This thesis aims to fill in the gap on Kv channels in small DRG neurons and deepen the understanding of their role in chronic pain, identifying the key subtypes, thus validating them as potential therapeutic targets.

This project focuses on the electrophysiological characteristics of K^+ currents in DRG neurons that have direct relevance to the study of chronic pain. In particular, I aimed to study the biophysics and pharmacology components of the currents that are directly involved in chronic pain process. Therefore, the overall goal of the present dissertation was to study alterations in Kv channel mediated currents in small DRG neurons from rat models of neuropathic (CCI of the sciatic nerve and STZ-induced PDN) and inflammatory (CFA-induced monoarthritis) chronic pain.

More specifically, this study aimed to:

1. Optimize and validate chronic neuropathic and inflammatory pain models through behavior tests, specifically with the quantification of mechanical hyperalgesia;
2. Identify the biophysical and pharmacologic patterns that are altered following induced CP, by the study of K^+ currents in small DRG neurons (derived from CCI, CFA and control rats) using voltage-clamp under whole-cell configuration;
3. Study the Kv channels expression, namely the expression of Kv1.3 and Kv1.4 isoforms (previously identified by electrophysiological studies), in DRG neurons derived from CCI neuropathic and CFA inflammatory rat models through Western assays.

Overall, results showed a development of hyperalgesia and an abnormal function and expression of Kv channels in small DRG neurons following neuropathic and inflammatory pain in rat models, contributing to their validation as potential targets for novel analgesics.

3. METHODS

3.1. Animal Pain Models

In the present work were used male and female Wistar rats with ages comprehended between 60 and 180 days. Three conditions have been studied – naïve control animals, procedure control (sham) animals and pain model animals, who were maintained for 4 weeks or 2 weeks after the procedure, depending on being neuropathic or inflammatory pain model, respectively. Animals were purchased from NMS|FCM and caged in a 12h light/dark cycle, at room temperature (21 ± 3°C) with water and food *ad libitum*. Animal care and experimental studies were in accordance with Directive 2013/63/EU, and the procedures were approved by the Ethical Committee of the NMS|FCM.

The animals were divided in four different groups: 1) chronic constriction injury (CCI), 2) complete Freund's adjuvant (CFA) and 3) painful diabetic neuropathy (PDN) and respective 4) naive controls. After establishment of the animal pain models, the onset of mechanical hyperalgesia was studied. Consequently animals were sacrificed for following harvesting of DRG ganglia. The biophysical properties of K^+ currents were studied by whole-cell voltage-clamp in up to 24h DRG neurons and protein expression of Kv channels in DRG ganglia was assessed by Western blot technique.

3.1.1. NEUROPATHIC PAIN MODEL: CHRONIC CONSTRICTION INJURY (CCI) OF THE SCIATIC NERVE – *CCI PAIN MODEL*

Ten female Wistar rats weighing initially 130–160g deeply anesthetized with ketamine/ diazepam in a proportion of 2:1 (100/5 mg/kg i.p.) prior to surgical exposure of the right sciatic nerve at mid-thigh level. The injury was performed as previously described (Austin et al. 2012) with collaboration of the plastic Surgeon Maria Angélica Roberto (PhD, MD) from the Centro Hospitalar de Lisboa Central EPE and a researcher from the lab (Joana Serrão, MSc).

The sciatic nerve of the right (ipsilateral) leg was accessed by the exposure of the mid-tight muscles by a blunt dissection with an iris scissor at the fascial planes. For a better access of the nerve, retractors were used. Four chromic gut (4.0, Catgut Chrom®) loose ligations were tied at the mid-thigh of the nerve. Suture of muscle was performed with

absorbable polyglycolic acid (5.0, Safil®) and suture of skin with soft silk (6.0, Silkam®) in both CCI and sham animals (Decosterd & Woolf 2000).

Sham animals had the nerve exposed and muscle and skin sutured in a way that no damage to the nerve was imposed.

Both naïve control (n=11) and sham (n=4) animals were age and weight-matched.

All the animals were let to recover after anaesthesia, one per cage. During the 4 weeks of development of the model, they were housed two littermates per cage.

3.1.2. INFLAMMATORY PAIN MODEL: COMPLETE FREUND'S ADJUVANT (CFA) INDUCED MONOARTHRITIS – *CFA PAIN MODEL*

Seven male Wistar rats (weighing initially 120-140g were deeply anesthetized with ketamine/diazepam (100/5 mg/kg i.p.) prior to the injection of 100 µL of complete Freund's adjuvant (CFA, Sigma F5881) medially between patella and femur-tibia junction (n=7). The right knee joint (ipsilateral) was gently rubbed around 50 times in a circular manner. Seven naïve rats were used as controls: the only procedure performed with this rats was using anaesthesia as the CFA ones; no other injection was applied, as any injection on the knee joint may induce inflammation by itself. This procedure was performed together with the researchers from the laboratory, Joana Serrão (MSc) and Marisa Sousa (PhD).

All the animals were let to recovery after anaesthesia one per cage. During the 2 weeks of development of the model, they were housed two littermates per cage.

3.1.3. DIABETIC PAIN MODEL: PAINFUL DIABETIC NEUROPATHY (PDN) – *PDN PAIN MODEL*

Five adult female Wistar rats weighing 100–180 g were injected with streptozotocin (STZ; 65 mg/kg i.p.) in the lower right quadrant of abdomen (Wu & Huan 2008; Carozzi et al. 2013) diluted in saline solution. Within 72h of injection, rats become hyperglycemic,

lowered glucose-stimulated insulin secretion and decreased glucose intolerance. In this regard, it is provided water with 5% sucrose, which is refilled every 12-24h for 3 days. The cage bedding is changed every 24-36h.

The induction of diabetes was assessed by biweekly measurement of the tail vein blood glucose level using a commercial blood glucose meter. Rats were considered hyperglycemic when blood glucose levels measured more than 300 mg/dL.

During the 4 weeks of development of the model, they were housed two littermates per cage.

3.2. Animal Behaviour

Before the procedures to induce and establish the pain models, animals were submitted to one week of habituation to the equipment and the operator. The operator was blind for each group (naïve and pain model) of rats, when possible. A baseline for mechanical sensitivity was obtained in the last three days of the habituation week. Behaviour tests were performed between 2 and 5 p.m. at the same weekday, for the entire course of establishment of the pain models.

3.2.1. SPONTANEOUS PAIN

During the first two minutes of habituation, before the mechanical hyperalgesia testing, the number of vertical activity (rear ups) in the open field of the behavioural cage was quantified, which consists in the number of times the rats rose up to an upright position. This movement was only accounted for when the rat stood vertically, both legs stretched and heels off the ground. The observation of the number of vertical rearings performed by rats in the open field of the behavioural cage is a putative approach to assess the innate responses to spontaneous pain (Rutten et al. 2014).

The baseline was measured for the three days prior to the procedure. Measurements were also performed on the 3rd, 7th, 14th (for CFA and for CCI), 21st and 28th day (for CCI) after the procedure to evaluate the progression of spontaneous pain throughout the establishment of the respective pain models.

3.2.2. MECHANICAL SENSITIVITY

Mechanical nociceptive thresholds were assessed using calibrated von Frey monofilaments (vFF) (Bio-VF-M, Bioseb®) by measuring withdrawal thresholds to an increasing pressure stimulus placed onto the medial plantar surface of the paw.

All animals were let to habituation for 15-20 minutes in the behavioural cage until cage exploration and grooming activities ceased (Chaplan et al. 1994). The behavioural cage is a transparent acrylic box with a thin grid floor (see Figure 10 below).

Figure 10 Behavioural cage with 4 Wistar rats during habituation period and von Frey filament stimulation for mechanical sensitivity. During the first two minutes of habituation, before the mechanical hyperalgesia testing, the number of vertical rearings in the open field of the behavioural cage was quantified, which consists in the number of rear ups that rats performed. Fifteen minutes later, mechanical sensitivity testing was performed by presenting the same von Frey monofilament 5 times, or until getting two positive painresponses.

Next, each monofilament (from 0.6 to a maximum of 26g) was presented 5 times for a maximum period of 5 seconds or until a withdrawal response was observed, with at least 5 seconds of interval between measurements (Hulse et al. 2011). This was repeated to both ipsilateral and contralateral leg. The threshold was taken as the first filament that elicited three pain responses (i.e., paw withdrawal, shaking or licking the paw).

The baseline was measured for the three days prior to the procedure. Measurements were also performed on the 3rd, 7th, 14th (for CFA and for CCI), 21st and 28th day (for CCI) after the procedure to evaluate the establishment of the respective pain model.

3.3. DRG neurons extraction and maintenance

All procedures were performed in accordance to previous work of the group (Serrão, 2015). Rats were overdosed with sodium pentobarbital (100 mg/kg i.p.) and sacrificed by decapitation. DRG harvesting was performed similarly to the described by Malin et al., 2007. Briefly, once the animal is in a prone position, using an iris scissors, a large transverse cut in middle of back skin was made in order to expose cervical, thoracic and lumbar spinal regions. A laminectomy was performed all the way to the caudal end of the rat to remove the roof of the vertebral canal and expose the spinal cord and DRGs: with a Littauer bone cutting forceps, a transversal cut was performed in the backbone at the lumbar L1 level; the spinal cord was exposed by cutting with the tip of the Littauer bone cutting forceps, one vertebra at the time, from one side of the vertebra canal to the other. To remove lumbar DRGs, the spinal cord and dura mater were pulled away from the inside of the backbone gently with the tweezers to expose the roots of the DRGs. Gently pulling with a set of tweezers, the DRGs were pulled out of the vertebral canal to be accessible to the spring scissors cut nerves and connective tissue. The DRG ganglia from L4 to L6 (for the neuropathic models) or L3 to L5 (for the inflammatory model) were removed one at the time and separated by right and left side.

All harvested ganglia was immediately transferred and dissected in four equal pieces in cold Krebs dissociation solution consisting of: NaCl 120 mM, KCl 5 mM, PIPES 20 mM, $CaCl_2$ 1 mM, $MgCl_2$ 1 mM and glucose 25 mM saturated with oxygen, pH 7.4, titrated with NaOH. Next, all ganglia was incubated for 45 minutes at 32°C in collagenase 3 $mg \cdot mL^{-1}$ (type IA, Sigma C9891) prepared in Krebs dissociation solution. The pieces of DRG ganglia were mechanically dissociated with a fire-polished Pasteur pipette at 20 minutes of digestion and at 45 minutes were dissociated again with a smaller-diameter pipette. By that time, trypsin was added to a final concentration of 2.5 $mg \cdot mL^{-1}$ (Sigma T9201). 40 minutes after digestion, an additional mechanical trituration was performed with an even smaller diameter fire-polished Pasteur pipette; 1.5 mL of Krebs dissociation solution was added to the cell suspension which was centrifuged for 5 minutes at 2000 rpm at room temperature.

In a laminar flow chamber, the dissociated DRG were plated in DMEM medium supplemented with 10% FBS and 1% penicillin-streptomycin. Neurons were maintained to a maximum of 24h in an incubator at 37ºC, 5% CO_2 with controlled humidity.

3.4. Electrophysiology

Membrane currents were recorded in *whole-cell voltage-clamp* configuration in isolated small DRG neurons, at room temperature (20-24°C), bathed in external solution (NaCl 135mM; KCl 5.4mM; $CaCl_2$ 2mM; $MgCl_2$ 2mM; HEPES 10mM; $D(^+)$-glucose 25mM; pH 7.4 titrated with NaOH; 310mOsm). It was used an electrometer (*Axon Instruments*, Axopatch 200B), an analogue/digital signal converter (*Axon Instruments*, DigiData 1200) and Clampex 6.0.3 (*Axon Instruments*) software.

The microelectrodes (2.0 - 3.8 MΩ) used were produced by a vertical pipette puller (Science Products GmbH, GB150T-8P) from borosilicate glass tubes (Science Products GMBH) were filled with internal solution (KF 140mM; $MgCl_2$ 1mM; $Na_{1/2}$-HEPES 10mM; EGTA 10mM; $CaCl_2$ 1mM; Na_2ATP 2mM; Na-GTP 0.4mM; pH 7.2–7.3 titrated with KOH; 300mOsm).

The liquid junction potential occurs when two solutions of different concentrations are in contact with each other. The more concentrated solution will have a tendency to diffuse into the comparatively less concentrated one. The rate of diffusion of each ion will be roughly proportional to its speed in an electric field. The liquid junction potential for internal and external K+ solutions is around 9 mV. Presented data is not corrected for junction potential.

A holding potential of -70mV was set and transients were immediately set to zero, currents were measured with capacitance compensation and series resistance compensation (80%), filtered at 10kHz, sampled at 5kHz, using a Digidata 1200 AC converter. Holding current and series resistance were monitored throughout all experiments.

3.4.1. VOLTAGE PROTOCOLS

Experimental conditions evoked K^+ currents by applying depolarizing pulses through the whole-cell membrane with minimal disruption of other ions equilibrium).

Currents were elicited by the following voltage protocols, applied in whole-cell voltage-clamp configuration to small DRG neurons (15 -25 µM), which were visually selected by size with a graduate ocular:

Voltage Dependence of Activation Protocol: From a holding potential of -70mV, currents were evoked by a set of 14 command pulses from -80 to +50mV, in 10mV increments, lasting 1040ms with 30s intervals, so that the total protocol lasted 3min15s. Each command pulse was preceded by a hyperpolarizing prepulse (-120mV, 120ms) in order to remove channel inactivation (particularly those responsible for the fast-component).

Voltage Dependence of Inactivation Protocol: From the holding potential of -70mV, a prepulse lasting 1040ms is elicited to the voltage at which one intents infer about the voltage dependence of inactivation, followed by the command pulse (that lasted for 600ms) to a voltage where full activation is obtained (+10mV). In this study, the series of prepulses ranged from -140 to +10mV were tested, with an interval of 30s between each. This protocol allows to evaluate the potential in which the channels close the inactivation gate.

3.4.2. DATA ANALYSIS

The electrophysiology data was analysed with Clampfit 10.3 (Axon Instruments®) software, Microsoft Excel (Microsoft Office 2013 Professional Plus®), and Origin Pro 8 (Microcal Software®).

Voltage Dependence of Activation: Activation profiles are a representation of current as a function of voltage so it can be plotted. Activation profiles can be transformed in ionic conductance and current density, as explained below.

Conductance (GG**)** was calculated from the I_{fast} and the I_{slow} values (corrected to I_{leak}), according to the following equation:

$$G = \frac{I}{V_m - E_K}$$

Equation 1

in which $\mathrm{V_m V_m}$ stands for pulse voltage and $\mathrm{E_K E_K}$ for the K^+ equilibrium potential, calculated by Nernst equation ($\mathrm{E_K E_K}$=-83mV). The conductance results were normalized to their maximum value ($\mathrm{G/G_{max}\, G/G_{max}}$) and the voltage dependence of the current was described by the following Boltzmann equation:

$$G/Gmax = \frac{A_1 - A_2}{1 + e^{(V_{1/2} - V_m)/V_s}} + A_2$$

Equation 2

in which V_m is the pulse potential, $V_{1/2}$ is the potential necessary to activate half the channel population, V_s is the slope constant (represents the equivalent number of charges that move in the membrane voltage field to cause the channel opening (Standen et al., 1987)) and A_1 and A_2 are the curve amplitude minimum and maximum, respectively.

To study the voltage dependence of steady-state inactivation, the fraction of channels available for activation is found by normalization of the currents obtained at the command pulse to its maximum value ($I/Imax$). Values of normalized currents were plotted against prepulse potentials, and data points from each cell were fitted with a sum of sigmoid functions, as described in the following equation:

$$I/Imax = \frac{A_1}{1 + e^{(V_{1/2fast} - V_m)/V_{Sfast}}} + \frac{1 - A_1}{1 + e^{(V_{1/2slow} - V_m)/V_{Sslow}}}$$

Equation 3

where $V_{1/2fast}$ and $V_{1/2slow}$ are the half-activation potentials of the fast and slow components of steady state inactivation of K^+ currents and V_{Sfast} and V_{Sslow} are the corresponding slopes and A_1 is a fitting parameter.

As stated previously, ion channels regulate the flow of ions across the membrane in all cells, which elicits an ionic current. **Current Density (**JJ**)** is measured in pA/pF, that is, current divided by capacitance, which doubles as a measurement of membrane area. The capacitance of the patch remains unchanged by the molecules that form the membrane so it is often regarded as constant (Cm=1µF/cm2) and hence proportional to the surface area of the cell (Sherman-Gold, 1993). Values of whole-cell capacitance were directly taken from the amplifier after current transients (Sherman-Gold, 1993). Current Density was calculated as in:

$$J = I \times C$$

Equation 4

where J J is current density (pA/pF), I is current (pA; elicited current from every depolarizing pulse of the voltage-dependence of activation protocol) and C C is capacitance (pF).

3.4.3. STATISTICAL ANALYSIS

Statistical analysis was performed with SigmaStat 3.5 (Systat Software Inc®). Samples were compared with Mann-Whitney rank sum test (nonparametric test that compares the distributions of two unmatched groups), when samples did not have a normal distribution and by the parametric t-test. When pertinent, it was also used the one-way ANOVA test. It was considered the following levels of significance: not significant (ns, $p > 0.05$) and significant (* $p \leq 0.05$, ** $p \leq 0.01$).

Presented results are described as mean ±S.E.M (standard error of the mean) for *n* samples.

3.5. Protein Expression

3.5.1. WESTERN-BLOT

Dissected DRG ganglia were placed immediately in cold homogenization buffer (HB) containing: EDTA 1mM, Tris 50 mM, NaCl 150 mM, pH 7.4 titrated with NaOH; and a protease inhibitor cocktail (PIC, ROCHE®, Basel, Switzerland, according to the manufacturer instructions) at the proportion of 10 mg of tissue to 100µL of HB^{+}PIC and stored at -80°C until required to processing.

Samples were homogenized with a manual homogenizer and incubated on ice for 30 to 40 minutes with lysis buffer (LB) 1% (w/v) sodium deoxycholate (DOC), 1% (w/v) nonited P-40 and 0.1% (w/v) sodium dodecyl sulphate (SDS). The lysate was centrifuged for 30 minutes at 12000 rpm, at 4°C and the supernatants were collected.

Total protein content was determined by the bicinchoninic acid (BCA) protein assay kit (Micro BCA Pierce Thermo®, 23235). Total protein extracts were denaturized in Laemmli sample buffer containing (in % w/v): dithiothreitol (DTT) 0.77, Bromophenol Blue 0.01, glycerol 5, SDS 1.5 and TRIS-HCl (pH 6.8); by mixing in vortex and incubating 10 minutes at room temperature. 30 µg of total protein extracts were separated by 7% polyacrylamide-SDS gel electrophoresis and electrotransferred to nitrocellulose membrane. These were blocked by TBS containing 5% non-fat milk and 0.1% Tween-20, and then incubated overnight at 4°C with the following primary antibodies: polyclonal rabbit anti-Kv1.4 (at dilution of 1:1000, Alomone labs® APC-007), polyclonal rabbit anti-Kv1.3 (at dilution of 1:1000, Alomone labs® APC-019) (Ritter, D.M. et al*.*, 2015) and as a loading control, the monoclonal mouse anti-α tubulin (1:2000, Santa Cruz® SC 58666). Following washes with TBS containing 0.1% Tween-20, the blots were incubated for 90 minutes at room temperature with the following Horseradish Peroxidase (HRP) conjugated secondary antibodies: polyclonal goat anti-rabbit (1:3000, Rockland® 611-1302) or with the secondary antibody polyclonal goat anti-mouse (1:3000, Rockland® 810-1102), depending on the host species of the primary antibody. Membranes were washed in TBS containing 0.1% Tween-20 and incubated with enhanced luminol chemiluminescence reagents (Clarity ECL Bio-rad®) according to the manufacture instructions.

The intensity of the signals was detected in a Chemidoc Molecular Imager (Chemidoc, BioRad®) and densitometry was performed using the Image Lab software

(BioRad®). Densitometry measures obtained from Kv1.3 and Kv1.4 protein lanes were normalized to the loading control and compared in terms of fold increase of expression in relation to the expression of L4-L6 or L3-L5 DRG neurons, depending on the pain model.

4. RESULTS

The findings of the present project point out for key protagonists of neuronal K^+ current changes, as well as for the underlying Kv channels, during CCI and CFA induced chronic pain.

4.1. Animal Behaviour

To characterize each rat pain models and their viability, two behavior read-outs were used and quantified. Namely, throughout the time span of the pain models spontaneous pain and mechanical sensitivity were monitored. Data was compared in three groups, regarding neuropathic and inflammatory chronic pain: 1) ipsilateral (injured/operated) CCI hind paw against contralateral (uninjured/internal control) CCI and Sham ipsilateral hind paws; 2) ipsilateral CFA hind paw against contralateral CFA and ipsilateral sham hind paws; 3) ipsilateral PDN hind paw against contralateral PDN and ipsilateral sham hind paws. A total of 36 animals were used: Naive (n=20) CCI (n=11); Sham (n=5); CFA (n=7); PDN (n=5).

Regarding the PDN pain model, it is not going to be featured in this dissertation. The model was performed as described in the Methods section but the rats did not become hyperglycemic nor did they exhibit any pain symptom (spontaneous pain and mechanical sensibility remained stable throughout the four weeks of the model – data not shown). Although it was not successful, this experiment gave important indications for the future, on how successful induction of the condition may be achieved.

4.1.1. SPONTANEOUS PAIN

As aforementioned, spontaneous pain is a common consequence of chronic pain. Therefore, the development of spontaneous pain was assessed in all neuropathic (CCI), inflammatory (CFA) and diabetic (PDN) pain models. This was quantified as the vertical activity (rearing; rear up) that rats performed in open field (on the behavioural cage). In chronic pain condition, it was expected to observe a reduction in the number of times that injured rats (CCI and CFA) reared up in open field, in comparison to their controls throughout the course of each model (Minett et al. 2014).

The vertical activity was accounted for and normalized to the last day of habituation, i.e. the last day before the procedure (surgery and injection).

4.1.1.1. CCI RATS SPONTANEOUS PAIN

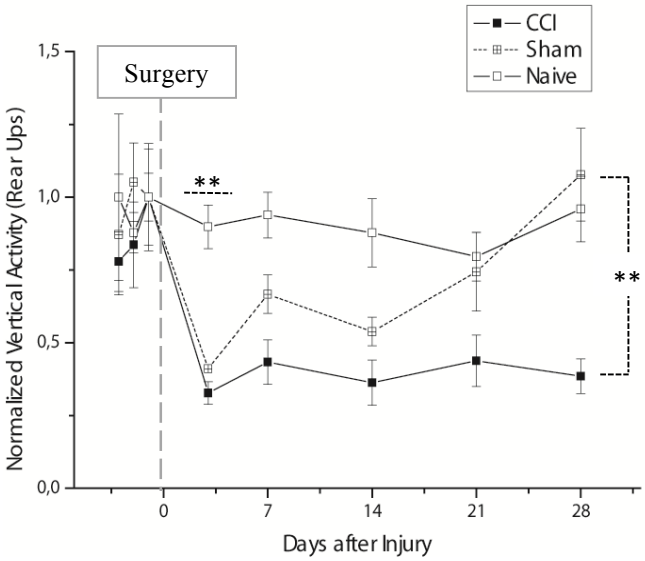

Figure 11 Counts of vertical rearings in an open field normalized to the last day of baseline from animals with neuropathic chronic pain. Normalized average of vertical activity from CCI rats (full line, black square, n=11), Sham (dashed line, crossed center square, n=5) and Naïve (full line, open square, n=10) rats obtained before and after injury. Error bars are given by S.E.M..

Looking at Figure 11, the baseline was well established, not showing much variation between the three days and between each group (difference of the mean is not statistically significant, $p>0.05$).

Regarding operates rats (both Sham and CCI) on the third day after surgery, their vertical activity decreased to 40% of its initial value whereas Naïve values remains constant throughout the 28 days.

CCI rats show a decrease in the number of rear ups by the third day after surgery, going from a baseline of 1±0.12 to 0.32±0.04. On that day, the mean difference between values from Naïve and CCI is significant (**, $p<0.01$; t-test). This value continues to decrease throughout the 28 days of the experiment, progressing to 0.18±0.02, representing nearly 20% of the initial vertical activity. Comparing this CCI mean value to Naïve control, their difference is still different (**, $p<0.01$; t-test).

Considering the behaviour of the values obtained from Sham animals, on the third and fourth week after the surgery (day 21 and day 28) the mean value of the normalized vertical activity of CCI rats is different from Sham values (**, $p<0.01$; Mann-Whitney rank sum test). From day 14 onwards, Sham rats showed a gradual return to baseline (and naïve) values (the difference of the mean values were not statistically significant: n.s., $p>0.05$; Mann-Whitney rank sum test).

Following surgery, operated rats exhibited abnormal posture of the injured hind paw (toes held together and plantar-flexed and paw everted), as well as repeated shaking, guarding and licking of the injured hind paw also suggesting the presence of spontaneous pain (Austin et al. 2012; Attal et al. 1990; Kajander et al. 1996).

4.1.1.2. CFA RATS SPONTANEOUS PAIN

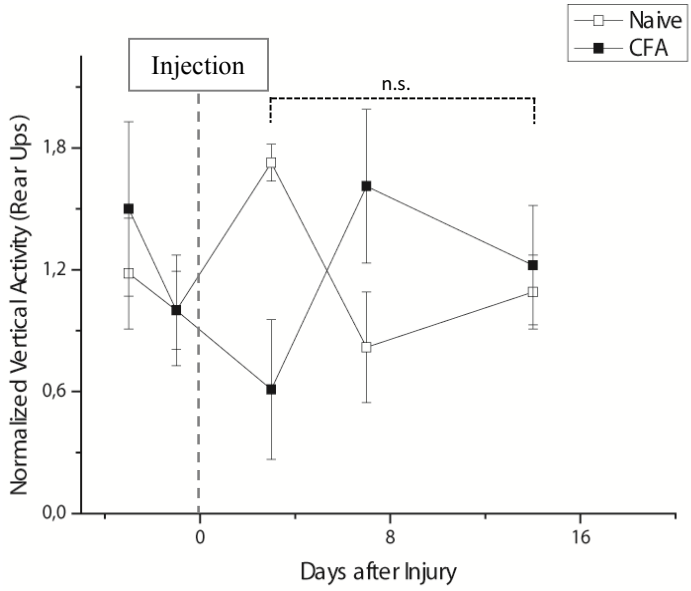

Figure 12 Counts of vertical rearings in an open field normalized to the last day of baseline from animals with inflammatory chronic pain. In CFA rats (black square, n=7) the average number of vertical activity was close to the average number of vertical activity performed by Naïve rats (open square, n=5) by the end of the model. Error bars are given by S.E.M..

Figure 12 that shows the normalized average number of vertical rearing in CFA rats is like the mean vertical rearing of Naïve rats during baseline (day -3 and -1). On day 3 after procedure, CFA rats presented a tendency to a lower average of vertical activity (n.s., $p > 0.05$; Mann-Whitney rank sum test) and this was only apparent on that day. In the following days, CFA rats recovered their vertical activity, surpassing Naïve and baseline values (difference of the mean not statistically significant, $p<0.05$; t-test). These results suggest that the CFA rats recovered from the procedure and the inflammation did not evolve to a chronic condition.

4.1.2. MECHANICAL SENSITIVITY

Another measurement carried out through the whole extent of the development and establishment of animal pain models was mechanical sensitivity. This was carried out by stimulating the ipsi- and contralateral hind paw of the pain model and Naïve rats using von Frey monofilaments (vFF) and quantifying withdrawal threshold. The mechanical threshold is defined as the weakest monofilament (g) that induced a pain behaviour in rats (Austin et al. 2012). Mechanical sensitivity is a direct measurement of primary and secondary hyperalgesia in the case of CCI and CFA rat models, respectively (Minett et al. 2014).

4.1.2.1. MECHANICAL SENSITIVITY IN CCI RATS

Mechanical sensitivity was assessed in CCI and Sham ipsilateral (injured) legs and Naïve right (control) leg. The CCI model produced a sustained and stable pain hypersensitivity for the whole experimental time-span after injury.

The contralateral (uninjured) legs of CCI and Sham rats and left Naïve leg were also accounted for (data not shown). No alterations in mechanical sensitivity were registered throughout the entire extent of the experiment.

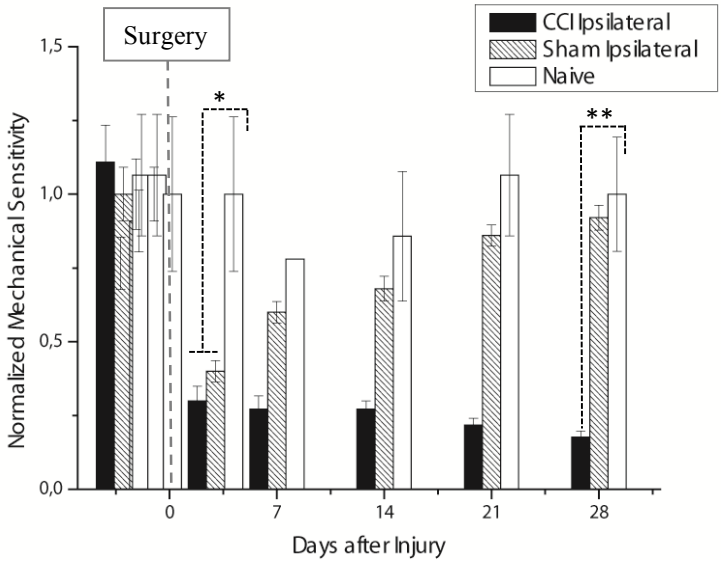

Figure 13 Sensitivity to mechanical stimulation as a measure of hyperalgesia in CCI pain models. The average withdrawal threshold of ipsilateral legs from CCI rats (black, n=11), Sham (black striped, n=5) and Naïve (white, n=10) rats are presented against the days before and after injury. Error bars are given by S.E.M.

Figure 13 represents the evolution of mechanical sensitivity of CCI, Sham and Naïve rats. After the surgery, CCI rats presented a lower withdrawal threshold when mechanical

stimulated (comparing with both Naïve and baseline values), reaching its minimum at the 28th day after injury. Sham rats showed their lowest withdrawal threshold at day 3 after surgery, showing recovering progression in the following days, until in the last day where it had the same threshold as the Naïve ones. The normalized average of mechanical sensitivity in Naive rats maintained its baseline value (1±0.26) all throughout the 4 weeks of the pain model (the mean difference of each day after surgery of Naïve rats was not statistically significant ($p>0.05$; one-way ANOVA).

Looking at the progression of mechanical sensitivity values in CCI rats one can note a clear reduction in the third day after surgery, a reduction of two thirds less than the naïve control (progressing from 1±0.12 at last day of habituation to 0.30±0.05). Such hypersensitivity persisted throughout all 4 weeks of the model. By the last day of the experiment, CCI values (0.19±0.02) were about 80% less than naïve (1±0.19) (**; $p<0.01$; t-test).

The results obtained from Sham rats show that the surgical procedure was not the cause of hyperalgesia development in the CCI group. By day 3 after the surgery, Sham rats had indeed a smaller mechanical sensitivity (0.4±0.04), showing a significant reduction of ~60% when compared with Naïve on the same day (1±0.26) (*, $p<0.05$, t-test). From day 7 onwards, Sham rats recovered from mechanical hypersensitivity, increasing it to levels comparable to Naïve ones by the end of the model (values of Sham results on days 21 and 28 are not statistically different when compared with Naïve values of the same day: n.s., $p>0.05$, Mann-Whitney rank sum test).

4.1.2.2. MECHANICAL SENSITIVITY IN CFA RATS

As in the previous assay, mechanical sensitivity was assessed in CFA ipsilateral leg and Naïve right leg. The CFA model evoked a transient increase of sensitivity but did not produce a stable lasting pain hypersensitivity.

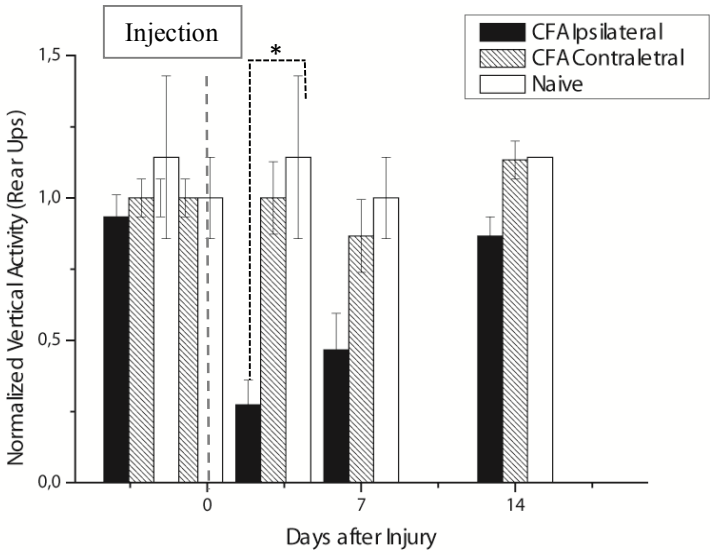

Figure 14 Sensitivity to mechanical stimulation as a measure of hyperalgesia in CFA pain models. The average withdrawal threshold of ipsilateral legs from CFA (black, n=7) and Naïve rats (white, n=5) and contralateral leg from CFA rats (black stripped, n=7) are presented against the days after injury. Error bars are given by S.E.M. (the differences between groups are not statistically significant: p>0.05 vs contralateral; t-test).

In Figure 14 the evolution of mechanical sensitivity of CFA and Naïve rats throughout the two weeks of the CFA pain model is presented. At the third day after the procedure, CFA rats presented their lowest withdrawal threshold when mechanically stimulated. From that day onwards, pain model rats showed a progressive recovery until, in the last day, threshold level as both their contralateral leg and Naïve controls were similar to control levels.

The normalized average mechanical sensitivity in Naïve rats maintained its baseline value (1.14±0.14) all throughout the 2 weeks of the pain model. At the last day of the experiment, Naïve rats measured a normalized average of 1.14±0.00. Looking at the CFA mechanical sensitivity in day 3 after the surgery (0.27±0.09), there was a reduction of about 75% when compared with its baseline values (1±0.07) and Naïve values of the same day (1.14±0.28). Such differences of the mean of CFA results in comparison with both baseline and Naïve values are significantly different (*, $p<0.05$; t-test).

Contrarily to CCI results, the CFA model did not produce a stable lasting pain. Instead, by day 7, the injected rats had already recovered to higher values of mechanical

sensitivity (0.47±0.13) as values no longer showed differences when compared with the respective Naïve of the same day (n.s., $p>0.05$; t-test). By the end of two weeks of the model, CFA rats showed the same threshold as both their contralateral leg and Naïve controls (CFA = 0.87±0.08; Contralateral Leg: 1.13±0.07; Naïve = 1.14±0.00; n.s., $p>0.05$; t-test).

The progression of mechanical sensitivity values throughout the experiment indicates that the rats did not develop secondary hyperalgesia in the "longer term", therefore, did not evolve into a chronic pain condition. These results on mechanical sensitivity, together with spontaneous pain results, allow us to infer that single-dose CFA injections are solely associated with transient inflammatory changes (Ren & Dubner 1999) and not with the evolution into a chronic condition.

4.2. Electrophysiology

4.2.1. WHOLE-CELL K^+ CURRENTS IN SMALL DIAMETER DRG NEURONS

The trace in Figure 15 is a typical K^+ current evoked by a +30mV depolarizing pulse (preceded by a -120mV prepulse) in a Naïve small diameter DRG neuron. Such currents are composed by a fast activation phase followed by a relatively fast current decay and a slowly inactivating current decay. Whole-cell K^+ current decay can be described as a summation of exponential functions, each describing either current component (Figure 15; see section 1.3.919). As aforementioned, currents are defined after the nature of the decay: a fast component (I_{fast}) and as a slowly inactivating component (I_{slow}). In this study, I_{fast} and I_{slow} were then measured as follows for each current sweep. The peak current was used as a measurement of I_{fast} and the I_{slow} was measured at the end of the command pulse (see Figure 17b).

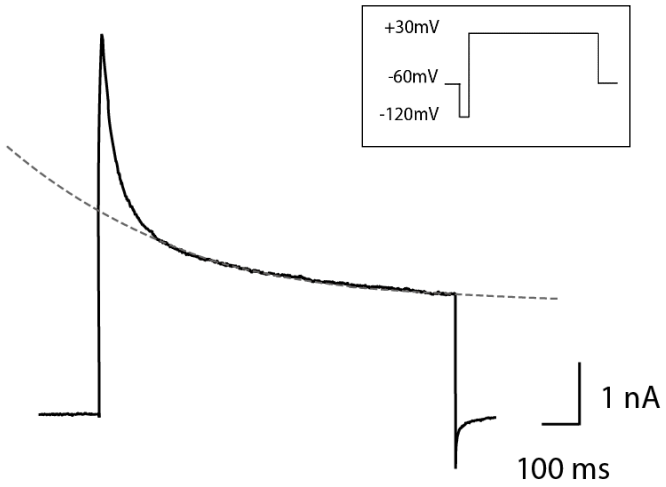

Figure 15 K^+ total current. This current is an average trace of all Naïve currents of small diameter DRG neurons obtained by a depolarizing pulse (+30 mV) applied from a holding potential of -60mV, preceded by a prepulse of -120mV, as shown on the top inset.

Figure 15 represents an average trace of all Naïve currents of small diameter DRG neurons obtained by a depolarizing pulse (+30 mV) applied from a holding potential of -60mV, preceded by a prepulse of -120mV, as shown on the top inset. The dashed line represents the exponential fit for the I_{slow} component. It is noticeable a great I_{fast} component in Naïve neurons, which can also be fitted by an exponential function.

As described below, each component has a different voltage sensitivity to inactivation. One can infer which current is more sensitive by applying the same command pulse at, for instance,+30mV varying only the prepulse (top inset, Figure 16). In Figure 16

one can depict that by applying a more hyperpolarized prepulse, such as at -120mV, one is allowing more channels to be available to conduct, removing them from the inactivated state.

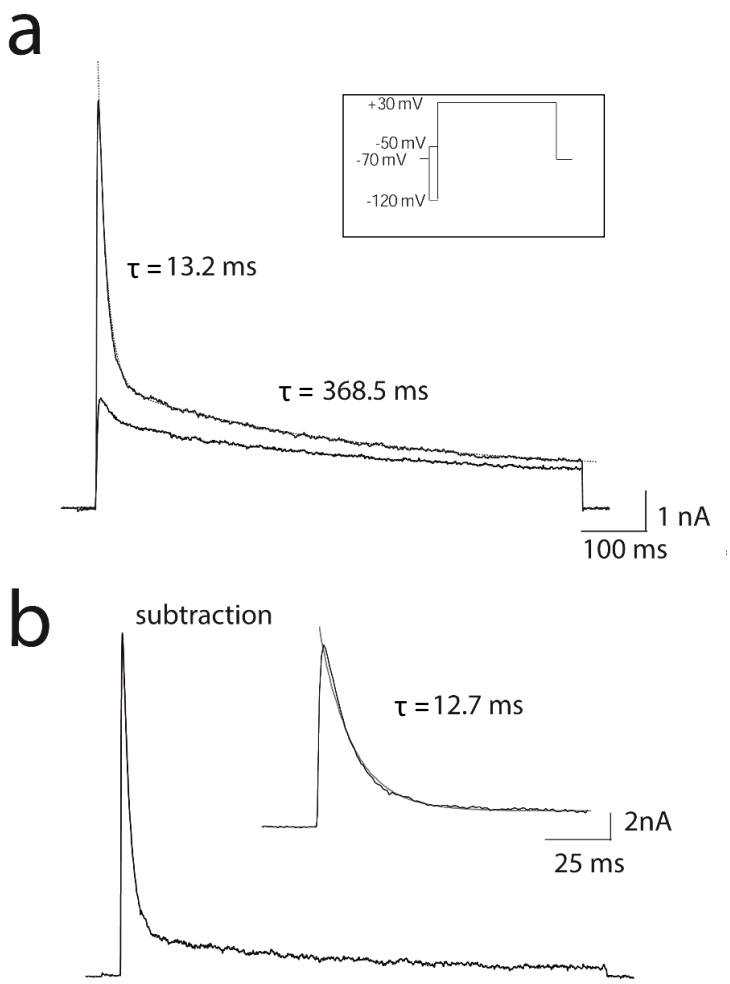

Figure 16 K+ whole-cell currents elicited by voltage protocol used to identify and characterize A-type currents. The command pulse to +30 mV was preceded by a prepulse either to -120 (see top insert). The consequent current traces are presented in 'a', the subsequent subtraction trace is presented in 'b'. The subtraction trace shows the fast, transient current with characteristics of A-type K^+ current.

Figure 16a. represents two currents, one elicited with a hyperpolarizing prepulse to -120mV and the other with a depolarizing prepulse to -50mV. Figure 16 b. depicts the resulting subtraction current, elucidating the voltage sensitive current. This resulting curve is characteristic of A-type Kv currents. As explained before, A-type currents are transient, fast inactivating currents that are very sensitive to voltage.

4.2.2. CURRENTS KINETICS IN SMALL DRG NEURONS FROM NAÏVE, CCI AND CFA RATS

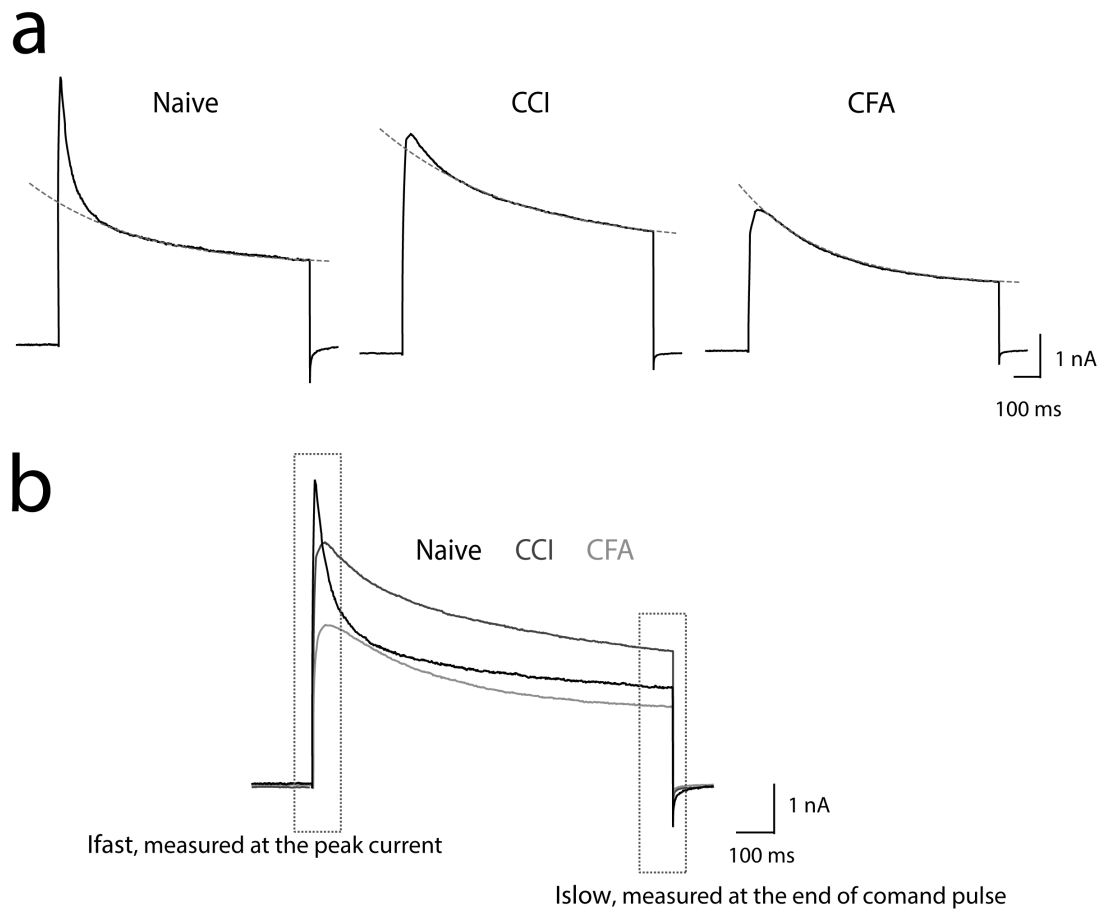

Figure 17 Averaged traces from voltage activated K^+ currents obtained from Naïve, CCI and CFA neurons. Currents were evoked by a command pulse +30mV, preceded by a prepulse of -120mV. A. Naïve (left, n=11), CCI (middle, n=9) and CFA (left, n=7) average current traces; **B.** Naïve (black), CCI (dark grey) and CFA (light grey) current traces plotted together for comparison.

Figure 17a. represents the average traces of Naïve (left, n=11), CCI (middle, n=9) and CFA (right, n=7). In Naïve condition, it is very noticeable two current components: I_{fast} and I_{slow} (as aforementioned). There is a clear difference between the I_{fast} and I_{slow} kinetics and, as seen on Figure 16 (also see Table 1). Naïve currents display an I_{fast} peak at around 9000 pA, whereas both CCI and CFA have a clear reduction of this component when compared to Naïve I_{fast} current component and to their I_{slow} current component.

Another obvious observation is the increase of the I_{slow} in CCI neurons, when compared with the Naïve average current. Differently from I_{fast}, this alteration in I_{slow} was only registered in CCI neurons, while CFA neurons remain within the range of values found

on Naïve neurons. This may be indicative of an underlying specific mechanism to neuropathic chronic pain.

The decay phase of K^+ currents recorded from small diameter DRG neurons (Figure 17 a.) was analyzed by fitting a sum of exponential functions in individual recordings. Time constants (τ) for each current component are presented in Table 1.

Table 1 Time-course of K^+ currents (kinetics). Pool data from n cells. The significant differences between the two pain models and naïve small diameter DRG neurons. τfast and τslow refer to the fitted exponential function time constants. The values are presented as mean ± S.E.M..

	τ_{fast}	τ_{slow}
Naïve *(n=13)*	32.57±2.63	468.03±52.68
CCI Ipsilateral *(n=11)*	109.17±41.92	398.73±50.81
CFA Ipsilateral *(n=8)*	N/A	363.43±27.98

As to the CCI currents (Figure 17, dark grey line), results showed that I_{fast} is slower in small DRG neurons ($\tau_{fastCCI}$ = 109.17 ± 41.92ms; n=7) than in Naïve ones ($\tau_{fastNaive}$ = 32.57 ± 2.63ms; n=11). This difference is statistically significant (*; p≤0.01; t-test) which means that neuropathic chronic pain primary afferents show an I_{fast} much less expressed and with slower kinetics. No significant differences were observed in the slow component kinetics (n.s.; p≥0.05; t-test) between CCI and Naïve currents. It is noticeable a notorious increase in current density on steady-state current of CCI neurons.

Focusing now on CFA results (Figure 17, light grey line), there are two main observations of crucial importance. The first one is that the I_{fast} component is not expressed. The CFA K^+ current decay was better fitted by one term only and so, contrarily to Naïve and CCI currents, CFA did not exhibit a summation of two exponential functions. The second observation is that, much like what occurred on CCI results, there was no significant difference in the slow component kinetics (n.s.; p≥0.05; t-test), although τ_{slow} in CFA ($\tau_{slowCFA}$ = 363.43 ± 27.98; n=7) is faster than in Naïve K^+ currents ($\tau_{slowNaive}$ = 468.03 ± 52.68; n=11).

4.2.3. CURRENT DENSITY

Current density represents the amount of current passing through a normalized membrane, i.e.: current/capacitance ratio (pA/pF). In this context, the current values obtained for each voltage from Figure 18.a were converted into current density values and represented in Figure 18.b. Current density was addressed for each current component.

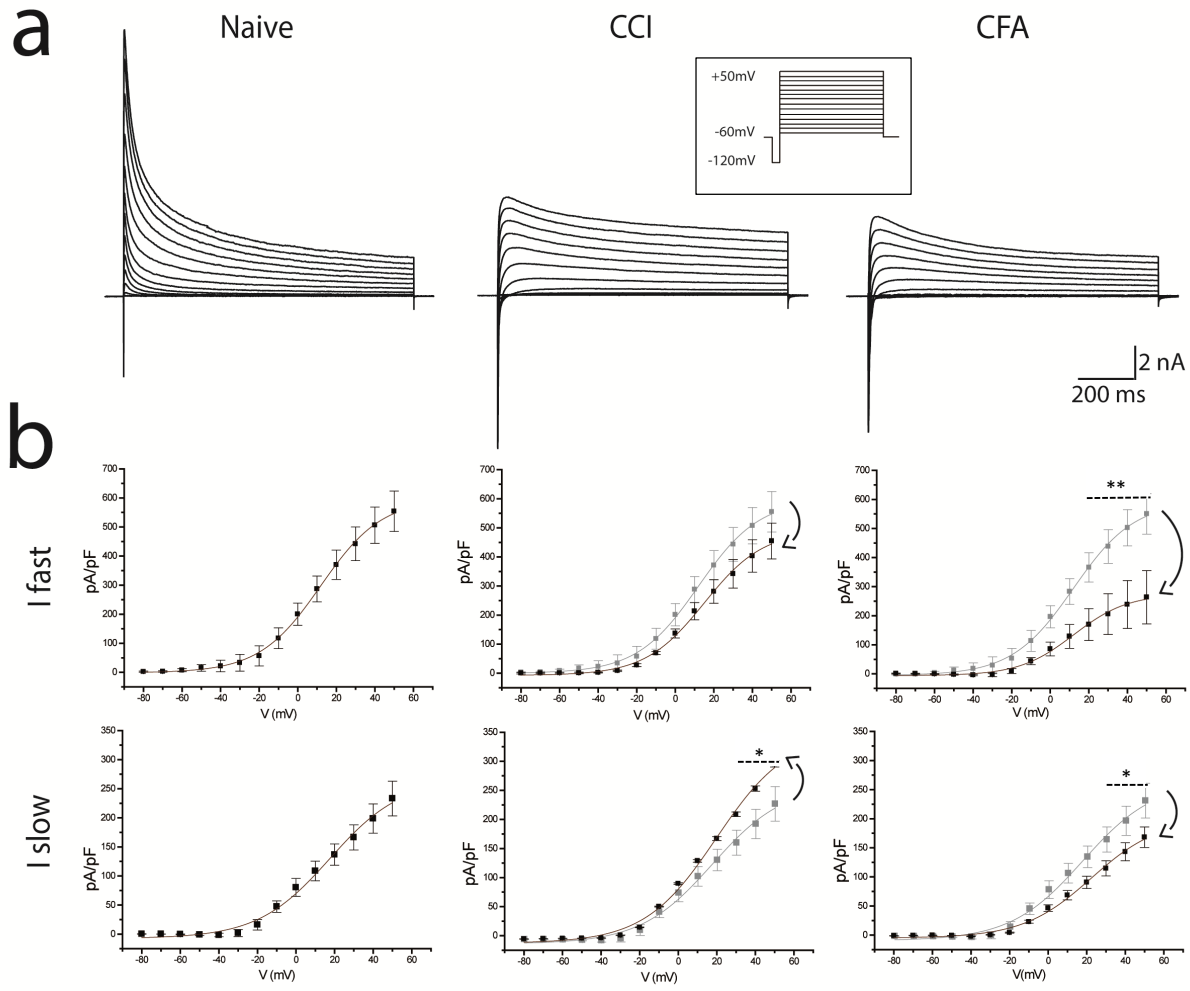

Figure 18 Voltage dependence of K^+ current density of small diameter DRG neurons derived from Naïve rats. K^+ current was normalized by cell capacitance as a measure of current density (pA/pF), solid lines are fits of Boltzmann functions to the average conductance values for a better comprehension of data. **a.** Average current traces of the activation profiles for Naïve (left), CCI (middle) and CFA (right) K^+ currents of small-diameter DRG neurons obtained by the voltage protocol depicted in the top inset; **b.** Current Density (pA/pF) values against command pulse voltage for Naïve (left panel), CCI (middle panel) and CFA (right panel) neurons. Current Density values from Naïve neurons is reproduced in grey in CCI and CFA panels as reference for direct comparison. Error bars are given in terms of S.E.M

Figure 18 represents current traces elicited by a series of increasingly depolarizing pulses, as seen on the top inset, and the respective conductance of each current against the voltage they were elicited for all small diameter DRG neurons. The average value of Current Density for each voltage is represented by a black square with respective S.E.M..

In DRG neurons from Naïve rats, the average maximum Current I_{fast} Density ($CD_{Ifast\ Naive}$), at +50mV, is of 553.99 ± 72.65 pA/pF (n=12) and the average maximum $CD_{Islow\ Naive}$ is of 233.27 ± 38.36 pA/pF (n=11). Such values are presented in Table 2:

Table 2 Maximum Current Density values (pA/pF) measured at +50mV for Naïve, CCI and CFA K+ currents of small diameter DRG neurons.

	Current Density Measured at +50mV (pA/pF)		
	Naïve	**CCI**	**CFA**
I_{fast}	533.99±72.65	454.77±61.73	263.49±97.68
I_{slow}	233.27±38.36	295.53±5.30	168.23±17.56

As previously seen on Figure 17, Naïve currents display a noticeable I_{fast} peak that in CCI is little expressed and in CFA is absent. Such reduction or abolishment of I_{fast} may be an underlying shared mechanism to both neuropathic and inflammatory pain.

Additionally, it was also identified an increase in I_{slow} component of CCI K^+ currents when compared with Naïve.

The following sections (4.2.3.1 and 4.2.3.2) are dedicated to the analysis of the nature of the alterations in currents found in both models, which require careful and separated analysis.

4.2.3.1. CURRENT DENSITY IN SMALL DIAMETER DRG NEURONS FROM CCI RATS

By observing the average current traces obtained from CCI neurons, it is obvious that I_{fast} is severely reduced when compared with the control. However, one must keep in mind that I_{fast} was measured at the peak of the current (Figure 17.b). Being whole-cell recordings, it is adequate to assume that I_{fast} and I_{slow} contributes to the value of peak current. So, with this method of quantifying current components, we were not able to quantify the obvious reduction of I_{fast} because, in parallel, there was an increase of I_{slow}.

In fact, that is why there is no significant differences observed between I_{fast} current density of CCI and Naïve neurons (see Figure 18.b, middle panel) (ns; p>0.05; t-test). Naïve neurons presented a maximum current density in I_{fast} current component of $CD_{Ifast\ Naive}$ = 533.99 ± 72.65 pA/pF, which was similar to what occurred in CCI neurons ($CD_{Ifast\ CCI}$ = 454.77 ± 61.73 pA/pF).

As suggested by direct observation of the obtained whole-cell current traces (see Figure 18.a), CCI I_{slow} component current density is increased ($CD_{IslowCCI}$ = 295.53 ± 5.30 pA/pF, n=9) when compared with I_{slow} derived from neurons of Naïve condition ($CD_{IslowNaive}$ = 233.27 ± 38.36 pA/pF, n=12) and this difference has statistical significance (*; p<0.05; t-test).

As mentioned, although the differential expression of I_{fast} is clearly noticeable between current traces obtained from Naïve and CCI rats, there is no statistical difference between Naïve and CCI current density of this component. In this regard, an alternative method for measuring I_{fast} was used by analyzing the isolated I_{fast} component of Naïve and CCI currents. The currents of most depolarized voltages (from +20mv to +50mv) were dissected in two exponentials and the I_{slow} was subtracted from the whole-cell current, resulting in the I_{fast} isolated (see Figure 19).

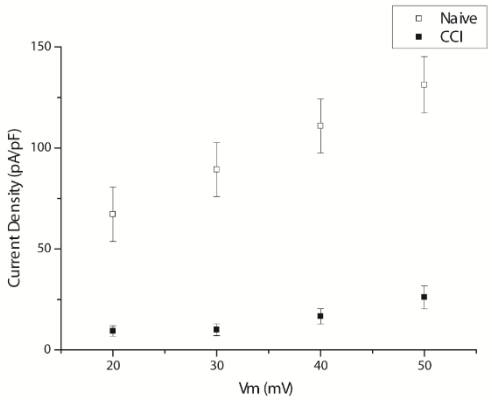

Figure 19 Naive and CCI isolated I_{fast} K^+ current density from +20mV to +50mV. To calculate the isolated I_{fast}, the currents of most depolarized voltages (from +20mv to +50mv) were dissected in two exponentials (each describing I_{fast} and I_{slow}) and the I_{slow} was subtracted from the whole-cell current, resulting in the isolated I_{fast}.

Like this, results of the isolated I_{fast} are in accordance with what is expected from observing whole-cell currents (see Figure 19). In the range of voltages +20mV to +50mV, where it is possible to dissect the two current components, one can observe the Current Density values are different at all potentials (**; $p<0.001$; t-test).

In resume, in neurons from CCI rats, I_{fast} is severely reduced and I_{slow} in enhanced when compared to currents recorded from neurons of Naïve animals

4.2.3.2. CURRENT DENSITY IN SMALL DIAMETER DRG NEURONS FROM CFA RATS

Regarding the I_{fast} component, the current density of CFA rats ($CD_{Ifast\ CFA}$ = 263.49 ± 97.68 pA/pF, n=7) showed values smaller than those from Naïve ($CD_{Ifast\ Naive}$ = 533.99 ± 72.65 pA/pF, n=12) with statistical significance (*, $p<0.01$, t-test) (see Figure 18.b, left pannel).

Looking at the I_{slow} component in Figure 18.b left panel, the current density of CFA rats ($CD_{Islow\ CFA}$ = 168.23 ± 17.56 pA/pF, n=7) shows no difference regarding Naïve values ($CD_{Islow\ Naive}$ = 233.27 ± 38.36 pA/pF, n=12) (n.s.; $p>0.05$; t-test).

Looking at data from CFA neurons, the fact that I_{fast} is reduced and I_{slow} remains unaltered suggests a higher state of neuroexcitability.

4.2.4. VOLTAGE-DEPENDANCE OF ACTIVATION: CONDUCTANCE

The activation profiles of the K^+ current components in small diameter DRG neurons of Naïve, CCI and CFA rats were assessed, by application of an activation protocol. As previously explained in section 3.4.1, this protocol is composed by a prepulse to -120mV to achieve full removal of inactivation before the stepping command pulses.

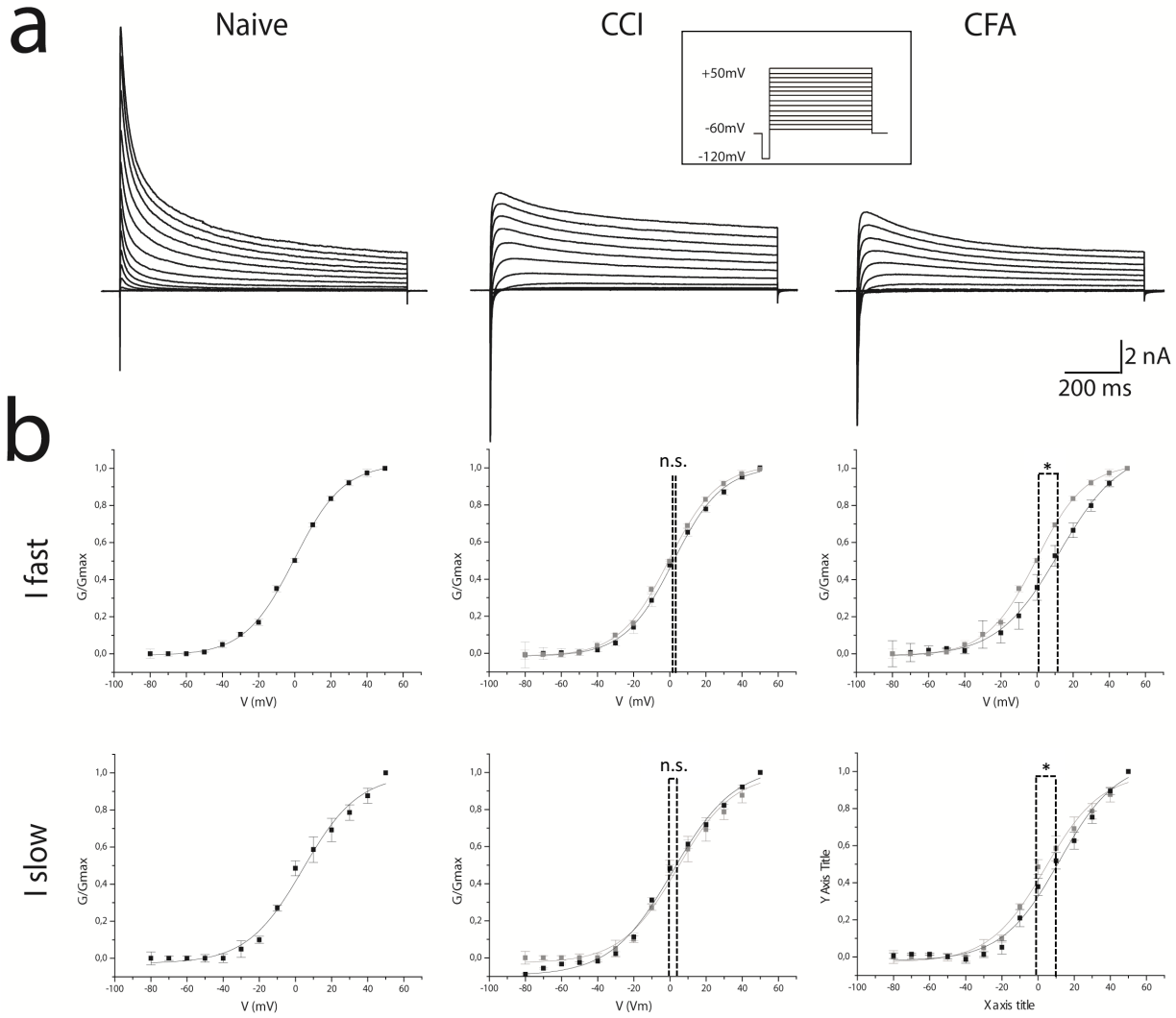

Figure 20 Voltage Dependence of Activation: K^+ current traces (a) and K^+ conductance/voltage relationship (b) of small-diameter DRG neurons obtained from Naïve, CCI and CFA rats. a. Average current traces of the activation profiles for Naïve (left), CCI (middle) and CFA (right) K^+ currents of small-diameter DRG neurons obtained by the voltage protocol depicted in the top inset. **b.** The Boltzmann function fit was simulated with the average experimental conductance values in order to better comprehend the tendencies. Conductance values from Naïve neurons is reproduced in grey in CCI and CFA panels as reference for direct comparison Error bars given by ±S.E.M..

The same average currents as Figure 19.a are presented in Figure 20, because the voltage protocol is the same. However, in Figure 20.b, data is treated differently. Here, data

is converted in conductance (G/Gmax). The average value of conductance for each voltage is represented by a black square with respective S.E.M.. The conductance/voltage relationships show the sensitivity of K+ currents to voltage for both Ifast (Figure 20.b, top) and Islow (Figure 20.b, bottom). The conductance/voltage relationships were better fit by a Boltzmann equation (Equation 2).

The fitting analysis indicated that the $V_{1/2}$ for the I_{fast} current in Naïve is 1.36±1.34mV and the V_S is 10.37±1.11mV (n=15). For I_{slow}, the $V_{1/2}$ is -0.79±2.26mV and the V_S is 12.48±2.00mV (n=15).

$V_{1/2}$ and V_S values were compared among the various profiles obtained from the different groups of small diameter DRG neurons, as follows on Table 3 (±S.E.M.).

Table 3 Voltage-Dependence of Activation: K^+ currents of small-diameter DRG neurons obtained from Naive, CCI and CFA rats. $V_{1/2}$ and V_S values are summarized after Boltazmann fit.

		Naïve	*CCI*	*CFA*
I_{fast}	**$V_{1/2}$**	1.36±1.34mV	2.01±1.10mV	12.54±1.68mV
	V_S	10.37±1.11mV	13.52±1.02mV	12.31±1.38mV
I_{slow}	**$V_{1/2}$**	-0.79±2.26mV	4.04±2.20mV	10.62±2.82mV
	V_S	12.48±2.00mV	15.52±1.89mV	17.93±1.99mV

The next two sections, activation profile parameters are compared and analyzed in detail.

4.2.4.1. VOLTAGE DEPENDENCE OF ACTIVATION IN CCI RATS

Results showed that recordings from CCI rats exhibited similar activation profiles to those of Naïve rats in both I_{fast} and I_{slow}.

Looking at the parameters of I_{fast} activation profiles, $V_{1/2}$ value of CCI K^+ I_{fast} currents ($V_{1/2Ifast\ CCI}$ = 2.01 ± 1.10mV; n=10) is not different from Naïve value ($V_{1/2Ifast\ Naive}$ = 1.36 ± 1.34mV; n=15) (n.s.; p≥0.05; t-test). Regarding the voltage slope, results for CCI ($V_{SIfast\ CCI}$ = 13.52 ± 1.02mV; n= 10) show a similar value when compared to Naïve ($V_{SIfast\ Naive}$ = 10.37 ± 1.11mV; n=15), once again not being statistically significant (n.s.; p≥0.05; t-test).

Parameters for I_{slow} activation profiles exhibit a similar pattern to I_{fast}. Differences observed in $V_{1/2}$ and V_S values are not statistically significant (n.s.; p≥0.05; t-test). $V_{1/2}$ value

of CCI K^+ I_{slow} currents ($V_{1/2Islow\ CCI}$ = 4.04 ± 2.20mV; n= 10) is similar to those of Naïve ($V_{1/2Islow\ Naive}$ = -0.79 ± 2.26mV; n=15). Regarding the voltage slope, CCI results ($V_{SIslow\ CCI}$ = 15.52 ± 1.89mV; n=10) show, once again, no differences with statistical significance when compared with Naïve values ($V_{SIslow\ Naive}$ = 12.48 ± 2.00mV; n=15) (n.s.; p≥0.05; t-test).

Altogether, results indicate that there are no differences in the voltage dependence of activation between currents of Naïve and CCI, since the voltage of half-activation of CCI neurons is similar to those of Naïve.

4.2.4.2. VOLTAGE DEPENDENCE OF ACTIVATION IN CFA RATS

Results from current traces of CFA neurons show significantly more depolarized activation curves (see Figure 20.b, left panel), suggesting a mechanism underlying the increase of excitability of neurons.

Looking at fitting parameters of voltage profiles of I_{fast} in CFA neurons (Figure 20.b, top, left panel), the $V_{1/2}$ value ($V_{1/2Ifast\ CFA}$ = 12.54 ± 1.68mV; n= 7) is more positive than those of Naïve ($V_{1/2Ifast\ Naive}$ = -0.79 ± 2.26mV; n= 15) (*; p<0.05; t-test). This results in a difference of about 12mV in the I_{fast} component (Figure 20). This finding indicates that rats with inflammatory pain display K^+ currents that are sensitive to more positive transmembrane potentials, whereas Naïve rats reach half-activation in more hyperpolarized voltages. Regarding the voltage slope, currents from CFA neurons ($V_{SIfast\ CFA}$ = 12.31 ± 1.38mV; n= 7) show no difference regarding values from Naïve neurons ($V_{SIfast\ Naive}$ = 10.37 ± 1.11mV; n=15) (n.s.; p≥0.05; t-test).

The voltage profile of I_{slow} has a similar pattern to I_{fast} (Figure 20.b, left, bottom panel). $V_{1/2}$ value of I_{slow} currents of CFA neurons ($V_{1/2IslowCFA}$ = 10.62 ± 2.82mV; n=7) is more positive than that of Naïve ($V_{1/2Islow\ Naive}$ = -0.79 ± 2.26mV; n=15) (*; p<0.05; t-test). This results in a difference of about 10mV in the voltage profile for the I_{slow} component (Figure 20.b, dashed lines). As stated above for the I_{fast} component, these results indicate that rats with inflammatory pain show less sensitivity to voltage. Regarding the V_S, currents from CFA neurons ($V_{SIslow\ CFA}$ = 15.94 ± 2.49mV; n=7) show no difference when compared to Naïve ($V_{SIslow\ Naive}$ = 12.48±2.00mV; n=15) (n.s.; p≥0.05; t-test).

Altogether, results from voltage profiles obtained from CFA neurons allow to infer that a given voltage stimulus, that is sufficient to activate the subjacent K^+ currents in Naïve DRG neurons, may be insufficient to activate currents in CFA neurons.

4.2.5. VOLTAGE-DEPENDANCE OF STEADY-STATE INACTIVATION

The study of voltage dependence of steady-state inactivation is used to assess the fraction of channels available for activation at determined membrane potentials. From the holding potential of -60mV, a prepulse is elicited at the voltage which one intent to infer the voltage dependence of steady-state inactivation (ranging from -140mV to +10mV), followed by the command pulse to a voltage where full activation is obtained (+10mV). Average current traces obtained from small DRG Naïve, CCI and CFA neurons are illustrated in Figure 21. Each current component is normalized to its maximum and plotted against voltage (Figure 21.b).

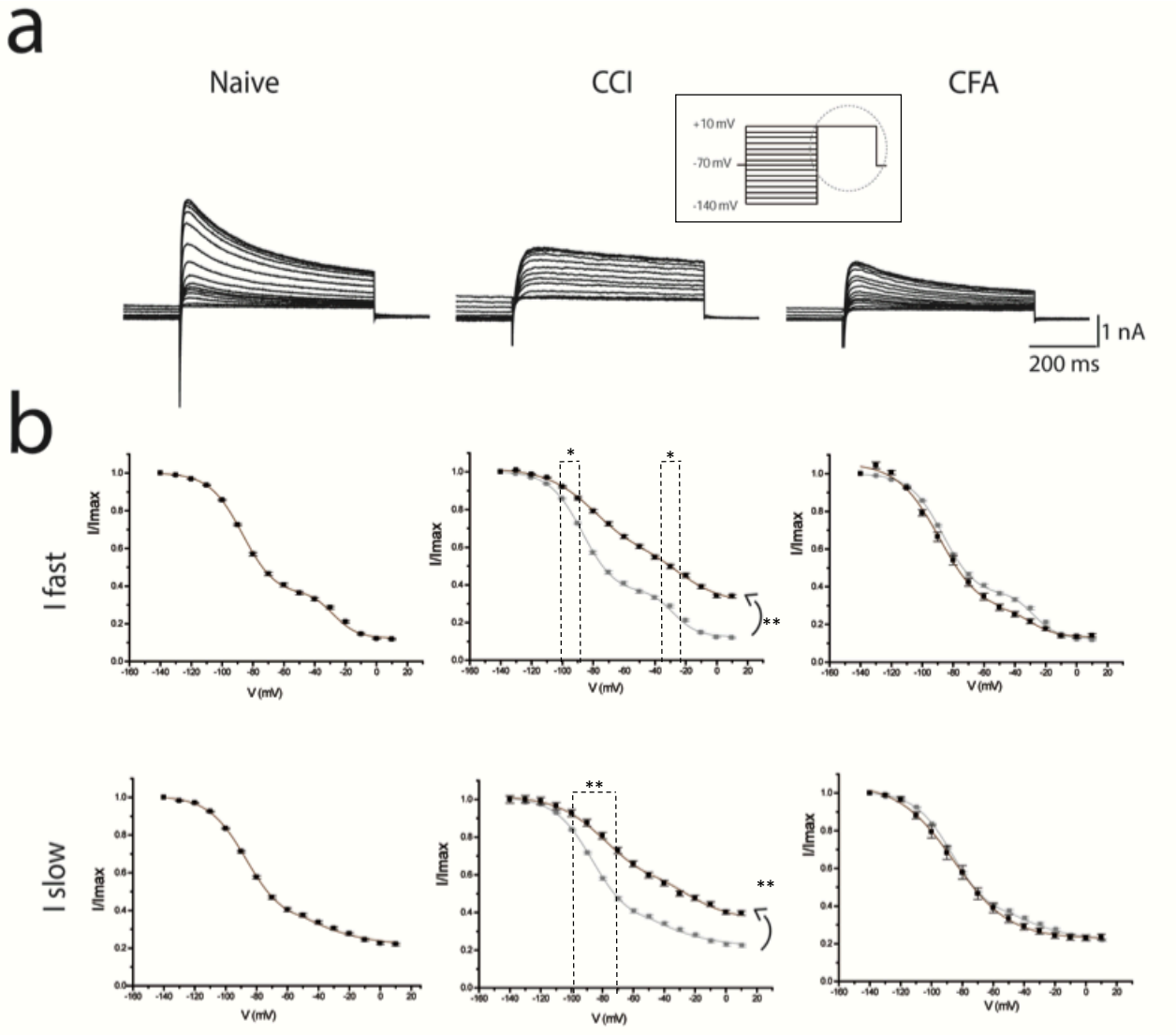

Figure 21 Voltage-Dependence of Steady-State Inactivation: A. Representative current traces from Naïve (left; n=11), CCI (middle; n=9), and CFA (right; n=7) DRG neurons when subjected to the protocol represented on the top inset. From the holding potential (-70mV), a pre-pulse ranging from -140mV to +10mV is elicited, followed by the command pulse to a voltage where full activation is obtained (+10mV). **B. Currents normalized to maximum value ($I/Imax$).** These values were obtained at the command pulse and plotted against the prepulse potentials. Average fitting parameters ($V_{1/2}$ and V_S) from the I_{fast} and I_{slow} components of inactivation are present in **Table 5**. Error bar are given to S.E.M..

Looking at the current traces from Naïve rats and respective current/voltage (I/V) relationships, it is visible, in both current components, a double inactivation period. There is one first component in the range of -140.V to -60/ -50mV (thereby defined here as *hyp*) and a second one between -60/ -50mV to +10mV (thereby defined here as *dep*). This last one is not so conspicuous for I_{slow}.

For the comparative analysis between profiles from Naïve, CCI and CFA, analysis was conducted in 3 different ways. Firstly, it was needed to look at what was happening in what the voltage shifts may represent in terms of current availability at a given voltage.

The difference between I_{fast} in CCI and Naïve measured at +10mV can be found in Table 4 and is significant, as at this voltage, CCI I_{fast} current is larger than Naïve ($I/Imax_{fast\ Naïve}$ = 0.118±0.004; $I/Imax_{fast\ CCI}$ = 0.340±0.023; **; p<0.001; t-test).

Table 4 Normalized Current measured at +10mV for Naïve, CCI and CFA K^+ currents of small diameter DRG neurons.

	Normalized Current Measured at +10mV		
	Naïve	**CCI**	**CFA**
I_{fast}	0.118±0.004	0.340±0.023	0.157±0.090
I_{slow}	0.221±0.007	0.397±0.011	0.235±0.015

This finding suggests that in a chronic neuropathic condition, at a given potential, there are less channels inactivated. This may also be indicative of a persistent current that was not present in Naïve condition. Naïve K^+ currents were about 90% inactivated at +10mV, whereas in CCI neurons currents only were 70% inactivated (Figure 21 b.).

I_{slow} current component from CCI neurons was equally distinct from that of Naïve. Indeed, I_{slow} in CCI currents were larger that Naïve currents at +10mV ($I/Imax_{slow\ Naïve}$ = 0.221±0.007; $I/Imax_{slow\ CCI}$ = 0.397±0.011; **; p<0.001; t-test). This, again, may also indicate a persistent current that was not present in Naïve condition. Naïve currents were about 80% inactivated at +10mV while CCI neurons only were 60%.

The inactivation profiles obtained for I_{fast} at +10mV were identical for both Naïve and CFA ($I/Imax_{fast\ Naïve}$ = 0.118±0.004; $I/Imax_{fast\ CFA}$ = 0.157±0.009; n.s.; p>0.05; t-test).

The inactivation profile obtained for I_{slow} was similar for currents from Naïve and CFA neurons +10mV ($I/Imax_{slowNaïve}$ = 0.221±0.007; $I/Imax_{slowCCI}$ = 0.235±0.015; n.s.; p>0.05; t-test).

These results suggest that the inactivation gating in neurons from CFA pain model is not affected by inflammatory pain.

A second perspective analysis on results of Figure 21 is to frame the data distribution with a fit of a single Boltzmann. Although the inactivating voltage profiles for I_{fast} current component Naïve neurons is better fit by a double Boltzmann function (as presented in Figure 21.b), the requirement for a two term Boltzmann function is not that clear for Islow current component from CCI or CFA neurons. Hence, a single Boltzmann was fit (or forced in same cases) to all voltage profiles (see Table 5) and considerations are of interest. The resulting $V_{1/2}$ and V_S were calculated through fitting a single Boltzmann function in normalized current to maximum current plotted against prepulse voltage. Table 5 summarizes the fitting parameters for K^+ currents of small-diameter DRG Naïve, CCI and CFA neurons.

Table 5 Average fitting parameters of inactivation profiles on small DRG neurons from Naïve, CCI and CFA model rats.

		Naïve	***CCI***	***CFA***
I_{fast}	$V_{1/2}$	-75.32±6.90mV	-55.52±4.67mV	-80.37±1.30mV
	V_S	24.07±7.05 mV	25.78±4.36mV	15.69±1.28mV
I_{slow}	$V_{1/2}$	-86.74±1.99 mV	-58.05±2.31mV	-82.82±2.95mV
	V_S	16.33±1.87 mV	17.76±2.16mV	13.58±2.84mV

The difference between $V_{1/2}$ values for Naïve and CCI for both I_{fast} and I_{slow} components is significant ($V_{1/2fast\ Naïve}$ = -75.32±6.90mV; $V_{1/2fast\ CCI}$ = -55.52±4.67 mV; *; p<0.05; t-test). Looking at the inactivation profiles (Figure 21), there is a visible shift of the inactivation curve to more depolarized voltages in CCI neurons.

An alternative third way to analyse these inactivation voltage profiles is to consider the two-stage inactivation. Table 6 shows the fitting parameters for $V_{1/2}$ and V_S for the two

terms of the inactivation voltage profiles (one more hyperpolarized, here termed *hyp*; and the second one more depolarized, here termed *dep*).

Table 6 Average fitting parameters of inactivation profiles on small DRG neurons from from Naïve, CCI and CFA model rats using a double-Boltzmann fit in peak current.

		Naïve	***CCI***	***CFA***
I_{fast}	$V_{1/2\ hyp}$	-88.73±2.10mV	-76.07±2.07mV	-50.03±12.82 mV
	$V_{S\ hyp}$	-9.17±0.87 mV	-5.57±4.02 mV	-55.86±28.50 mV
	$V_{1/2\ dep}$	-22.21±3.57mV	-10.25±1.50mV	-13.91±24.57mV
	$V_{S\ dep}$	-20.45±2.68mV	-28.56±8.15mV	-33.33±15.77mV

From the analysis of Table 6, one can note that $V_{1/2}$ values, for the more hyperpolarized inactivation curve (*hyp*), there is a depolarizing shift for both CCI and CFA neurons, when compared with values from Naïve neurons. Also, as seen from Table 6, CFA inactivation curve is not well fitted by a double Boltzmann function as S.E.M. values are very high. CCI and Naïve curve shifts are significant ($V_{1/2\ hyp\ \text{Naïve}}$ = -88.73±2.10mV; $V_{1/2\ hyp\ \text{CCI}}$ = -76.07±2.07mV; *; $p<0.01$; t-test) and greater than 10mV. Similar trend can be observed for the more depolarized "hump" (*dep*).

This means that, with nerve injury, currents become less inactive for a larger range of voltages. So, with K^+ current inactivation impaired, one can expect lower levels of excitability.

4.3. Western-blot

New evidence suggests a previously unacknowledged contribution of K^+ channels (especially A-type current channels, as Kv1.4, Kv3.4 and Kv4.3) in chronic pain processing. It has been given special attention to Kv1.4 as several studies have identified it as having its expression downregulated in chronic pain condition (Wells et al. 2007; Park et al. 2003; K Ishikawa et al. 1999; Rasband et al. 2001).

Also, from the previous studies (Ishikawa et al. 1999), there is evidence of Kv1.3, the main contributor to I_{slow} current component, is altered. The curious part is that Kv1.3 is seldom mentioned in chronic pain studies since it is not highly expressed in DRG neurons. When it is mentioned, it appears to be downregulated in chronic pain condition (Ishikawa et al. 1999; Du & Gamper 2013).

Here, the expression of the K^+ channels Kv1.3 and Kv1.4 were assessed in DRG ganglia and sciatic nerve from the CCI model by Western blot technique.

4.3.1. KV1.3 AND KV1.4 EXPRESSION IN NAÏVE AND CCI FROM L4-L6 DRG

Figure 22 shows the western blot and respective band quantification for immunoreactivity against Kv1.3 and Kv1.4, for DRG samples obtained from Naïve and CCI rats.

For the CCI pain model (n=3) and respective Naïve controls (n=3), after the quantification of the total protein content in L4-L6 DRG ganglia from the ipsilateral site of injury and right leg, respectively, samples of 30µg of total protein were analysed.

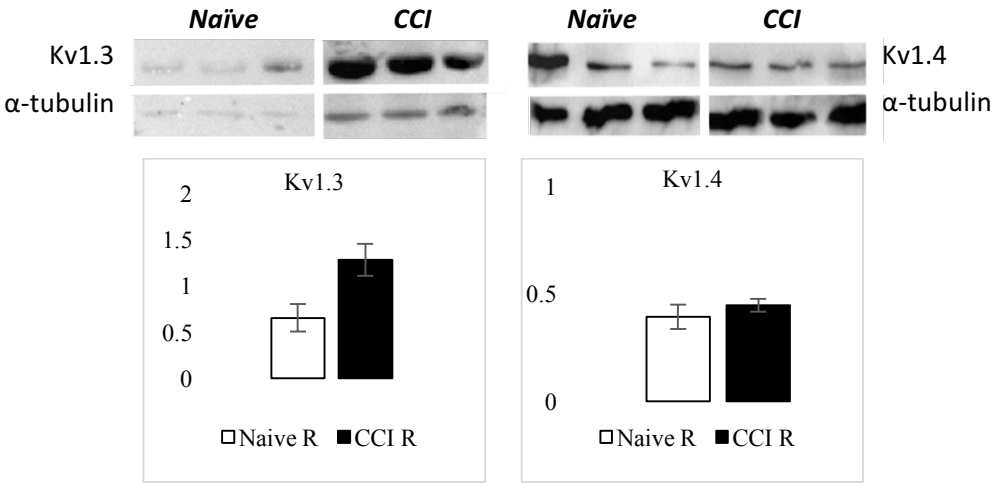

Figure 22 Expression of Kv1.4 and Kv3.4 proteins in DRG from CCI and Naive L4-L6 DRG. Top: results of the assessment of Kv1.3 and Kv1.4. α tubulin was used as the loading control. Bottom: quantification of the fold increase in protein expression of Kv1.3 (left) and Kv1.4 (right). Errors and error bars in sham are given in terms of S.E.M.

Representative blots from the samples tested are shown in Figure 22. After normalization to the internal loading control (α-tubulin, represented in the bottom panels), the following considerations regarding the results can be considered:

1. There is a significant increase in Kv1.3 expression in L4-L6 DRG of CCI rats (1.28±0.17, n=3) when compared to Kv1.3 expression in Naïve rats (0.65±0.15, n=3) (*, $p<0.05$; t-test);
2. There is no significant difference between values of Kv1.4 expression in CCI and Naive, although Kv1.4 (0.45±0.05, n=3) seems to be more expressed in CCI neurons (0.39±0.06, n=3) (n.s.; $p>0.05$; t-test).

Noteworthy, the n for each membrane and, therefore, for each consideration is 3 samples. This is a very small amount of sample that does not allow to take conclusions, as it merely points out some tendencies. Also, Kv1.4 overexpression does not follow accordingly electrophysiology results. It is expected to have downregulated A-type Kv channels as a possible cause of reduced expression of I_{fast} current component. On the other hand, these samples are of whole ganglia. Knowing Kv channels are transmembrane channels, it should be taken as a future direction repetition of these protein assays with plasma-membrane enriched protocols.

4.3.2. KV1.3 AND KV1.4 EXPRESSION IN NAÏVE AND CCI FROM THE SCIATIC NERVE

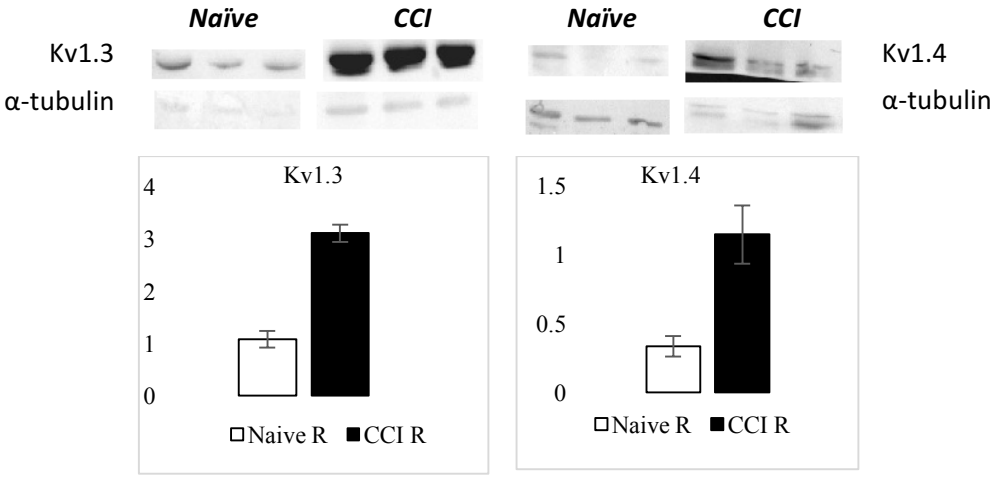

Figure 23 Expression of Kv1.4 and Kv3.4 proteins in DRG neurons from CCI and Naive sciatic nerves. Top: results of the assessment of Kv1.3 and Kv1.4. α tubulin was used as the loading control. Bottom: quantification of the fold increase in protein expression of Kv1.3 (left) and Kv1.4 (right). Errors and error bars in sham are given in terms of S.E.M.

Representative blots from sciatic nerve samples tested are shown in Figure 23. After normalization to the internal loading control (α-tubulin), the following results regarding Kv1.3 and Kv1.4 were obtained:

1. There is a significant increase in Kv1.3 (3.11±0.17, n= 3) expression in sciatic nerve when compared to Naïve Kv1.3 expression (1.07±0.16, n=3) (*, $p<0.05$; t-test);
2. There is an apparent increase of Kv1.4 expression in CCI sciatic nerve (0.34±0.07, n=3) when compared with Naïve nerves (1.15±0.21, n=3) but this is not significant due to the variation observed in Kv1.4 blots (Figure 23) (n.s. $p>0.05$; t-test).

Altogether, these results indicate that Kv channels are dynamic and are differentially expressed in the context of chronic pain.

5. DISCUSSION

The work developed throughout the past year gives valuable insights to the physiopathology of chronic pain. Briefly, both pain model rats exhibited altered behaviours in comparison to their controls and an impaired function and expression of K^+ currents and underlying Kv channels in small-diameter DRG neurons.

5.1.1. DID THE NEUROPATHIC AND INFLAMMATORY PAIN MODELS EVOLVE TO A CHRONIC CONDITION?

As aforementioned, spontaneous pain is a common consequence of chronic pain. Therefore, the development of spontaneous pain was assessed in all neuropathic (CCI) and inflammatory (CFA) pain models. This was quantified as the vertical activity (rearing; rear up) that rats performed in open field (on the behavioural cage). In chronic pain condition, it was expected to observe a reduction in the number of times that injured rats (CCI and CFA) reared up in open field, in comparison to their controls throughout the course of each model (Minett et al. 2014).

Regarding the neuropathic pain model, CCI rats showed a reduction on rear ups in injured rats, reduction that was maintained constant throughout the 4 weeks of the model after surgery. The results also showed a recovery of vertical activity to basal values (comparable to naive at the same time point) of Sham rats (operated, non-ligated sciatic nerve). These results suggest CCI rats experienced more spontaneous pain, compared to naïve and sham ones and allow to infer CCI maintenance of spontaneous pain is due to the loose ligations on the nerve and not because of the muscle and skin sutures (otherwise, Sham rats would also show a persisting smaller vertical activity).

As stated in section 4.1.1.1, following surgery, operated rats exhibited abnormal posture of the injured hind paw (toes held together and plantar-flexed and paw everted – data not shown), as well as repeated shaking, guarding and licking of the injured hind paw suggesting the presence of spontaneous pain (Austin et al. 2012; Attal et al. 1990; Kajander et al. 1996). Sham rats reverted normal posture of the injured hind paw by day 14 after the surgery whereas CCI rats continued exhibiting this behavior all throughout the course of the experiment. This reinforces the suggestion that chronic pain was obtained in the CCI model.

Regarding the inflammatory chronic pain model, CFA rats showed an erratic progression of vertical activity. CFA rats only presented a lower average of vertical activity (difference not significant) than Naïve controls at the third day after injection. The following days CFA rats recovered their vertical activity, surpassing Naïve and baseline values (difference of the mean was not significant). Also, Naïve values were not constant, oscillating throughout the 14 days of experiment. Similar observations suggest that, if any, pain was only evoked transiently in the few days following the CFA injection.

Another measurement carried out through the whole extent of the development and establishment of animal pain models was mechanical sensitivity. This was carried out by stimulating the ipsi- and contralateral hind paw of the pain model and Naïve rats using von Frey monofilaments (vFF) with different weight bending forces and quantifying withdrawal threshold. Mechanical sensitivity is a direct measurement of: primary hyperalgesia for CCI rat model, hence the elicited nerve is the injured one; secondary hyperalgesia in the case CFA rat model, hence the area stimulated and the area affected are not the same (Ren & Dubner 1999).

In the CCI neuropathic pain model, three days after injury, the average withdrawal threshold from ipsilateral hind paws of CCI rats was significantly lower in comparison to the withdrawal threshold of the naïve hind paws, revealing that CCI rats developed mechanical hyperalgesia. This higher sensitivity was maintained constant throughout the experiment and by twenty-eight days after injury (end of the progression of the pain model), the ipsilateral sensitivity of CCI rats showed its minimum withdrawal threshold. Once animals were sacrificed, neither an absorption of the chromic gut suture or a regeneration of the sciatic ipsilateral nerves from CCI rats were observed. These observations indicate that the higher sensitivity of CCI rats is due to the ongoing sensitization of nerve fibers.

Regarding both spontaneous pain and mechanical sensitivity read-outs for the neuropathic pain model, CCI rats maintained a posture described as pain behavior (Minett et al. 2014) and had high mechanical sensitivity (low withdrawal threshold) throughout the entire time span of the experiments. Sham rats had a similar behavior on both read-outs during the first week but developed to same behavior shown by Naïve rats in the last three weeks. Hence, the protocol used for the neuropathic pain model appears to be adequate to induce chronic pain behavior on rats.

In CFA pain model rats, the marked decrease in paw withdrawal threshold at the 3rd day post injury is a consequence of the development of secondary hyperalgesia. These results are corroborated with consistent observations from other researchers in a very similar inflammatory CFA pain model (Ren & Dubner 1999; Borzan et al. 2010). However, as the model progressed, the average ipsilateral hind paw sensitivity to pain from CFA rats recovered back to contralateral and naïve controls at the fourteenth day post-injury. Based on this behavioural development and on spontaneous pain results, it is possible to conclude that it was not possible to achieve chronic inflammatory pain with the protocol proposed for this model. However, it was possible to induce transient pain, as that by the third day after injection of CFA it was possible to observe acute pain.

As a future direction, it would be interesting to study at electrophysiological level the neuronal consequences of acute pain, terminating the model by the third day, according to the results. Also, previous studies showed that single-dose CFA injections are solely associated with transient inflammatory changes, not evolving to a chronic condition (Ren & Dubner 1999). It is also know that chronicity can be achieved by priming the knee with another inflammatory (for example, carrageenan) agent 5 days – 1 week prior to injection of CFA (Kidd & Urban 2001; Ren & Dubner 1999; Reichling & Levine 2010), which would be advisable to incorporate in the protocol for a better understanding of its physiopathology.

5.1.2. WHAT ARE THE FUNCTIONAL CONSEQUENCES AT THE NEURONAL LEVEL OF THE OBSERVED HYPERALGESIC BEHAVIOUR?

In order to access what are the consequences of the observed hyperalgesia phenomena, electrophysiological studies were conducted. The current running through a biological membrane depends on open channel probability and duration, open channel conductance and voltage-gated channel density (Bezanilla 2005). If one of these conditions is altered or impaired, physiopathology may occur.

5.1.2.1. IS THE VOLTAGE DEPENDENCE OF ACTIVATION IMPARED IN NEUROPATHIC CHRONIC PAIN?

The analysis of biophysical properties of K^+ currents in isolated small diameter DRG neurons showed I_{slow} current density to be increased in CCI neurons in comparison to Naïve ones. This increase in current density was not due to a change in the voltage dependence of activation. Conductance results show no difference when compared with Naïve rat neurons. As stated before, current depends on open channel probability, open channel conductance and voltage-gated channel density (Bezanilla 2005). Since the conductance does not appear to be impaired, and open channel probability is not assessed by whole-cell configuration, the difference between Islow current density from pain model and Naïve neurons may lie in the channel density, i.e. protein expression. This way, one may wonder if it is the Kv1.3 channel that is altered since it is the only Kv1 isoform that exhibits a C-type (slow) inactivation mechanism. Western-blot evidence presented suggests that the enhancement of I_{slow} in K^+ currents in neurons from CCI rats is due, at least in part, to an alteration in Kv1.3 over-expression in L4-L6 DRG. Since Western-blot assays were performed with the entire ganglia, it is not possible to state with accuracy if this increase is specific to small, medium or large DRG neurons. In this context, one should not disregard that Kv1.3 altered expression may not account for the biophysical difference observed between CCI and Naïve neurons. Further assays must be conducted in order to access the expression of Kv1.3 in the membrane of L4-L6 DRG through immunohistochemistry and Kv1.3 expression in plasma-membrane enriched Western-blot assays.

The observed increase in current density of the I_{slow} component and the overexpression of Kv1.3 in neurons from CCI pain model rats is not described in literature. In fact, it is described the exact opposite: Kv1.3 and I_{slow} component is often reported as decreased with pain, either on electrophysiological as on protein expression assays (Kim, Choi, Rim & Cho 2002; K Ishikawa et al. 1999; Mishra & Narayanan 2014; Zhang et al. 1997; Everill et al. 2014; Abdulla & Smith 2001). Upon activation, K^+ channels facilitate an extremely rapid transmembrane K^+ efflux that can influence action potential threshold, waveform and frequency. Because K^+ channel opening repolarizes (and even, hyperpolarizes) the neuronal membrane, this function can limit action potential generation and firing rate (Tsantoulas & McMahon 2014). A possible explanation for the increased current density of I_{slow} current component in CCI neurons lies in generation and accommodation of firing of action potentials. A larger K^+ current may lead to a more rapid repolarization of the membrane potential, which also means the resting membrane potential is reached relatively fast. So, this increase in I_{slow} should been looked at in combination, considering the marked decrease of Ifast. It has been shown that I_{fast} is typically involved in setting the interspike interval (Hille 2001), while I_{slow} is essential for fast repolarization of action potentials and consequently contributes to repetitive firing pattern (Armstrong 2003). So, as a results of such dramatic decrease of I_{fast}, one could expect firing frequencies that could lead to nerve firing failure. The increase of Islow may be the mechanism that allow sustain firing to persist over time, typical of a chronic condition. In this context, together with results regarding a faster recovery of voltage-gated sodium channels following inactivation (Serrão 2015), one can infer the membrane is able to accommodate higher firing frequencies, thus promoting a higher but sustainable neuroexcitability.

I_{fast} component is reduced in CCI pain model. Electrophysiological recordings demonstrated that this reduction in current density was not due to a change in the voltage dependence of activation. Conductance results show no difference in I_{fast} current component when compared with Naïve rat neurons. Once again, if the alteration is not at the voltage sensitivity, it probably is due to differential expression of the channels responsible for the I_{fast} current component. As previously stated, the main A-type Kv channel

in small-DRG neurons is Kv1.4. Having a reduction of I_{fast} K^+ currents in neurons from CCI pain model rats, it was expected to have a reduction in expression of Kv1.4. Thus, Kv1.4 expression was accessed in L4-L6 DRG by Western-blotting and there was no significant variation between CCI and Naïve ganglia. Although this result appears to be compromised by uneven internal control (α-tubulin), and is based on a very small sample (n=3), this result goes against what was expected and previously described (K Ishikawa et al. 1999; Park et al. 2003; Rasband et al. 2001). Once again, Western-blot assays were performed with the entire ganglia, so it is not possible to state with accuracy if these results are accurate regarding only small-diameter DRG neurons. In this context, one should not disregard that Kv1.4 unaltered expression may not account for the biophysical difference observed between CCI and Naïve neurons. It is actually likely that the shift in expression with nerve injury may just occur at the plasma membrane, corresponding in a fast cell surfacing phenomena. Further assays must be conducted in order to access the expression of Kv1.4 specifically in the membrane of L4-L6 small-diameter DRG neurons through immunocytochemistry and plasma-membrane enriched Western-blot assays.

Peripheral nerve injury triggers a wide variety of cellular changes in DRG sensory neurons. Under physiological conditions, K^+ currents contribute to the suppression of action potential generation, and thereby suppress neuron excitability. Therefore, a reduction in Kv channels and hence Kv current, by either injury or pharmacologic agents, should result in increased neuronal excitability. In DRG neurons large reductions in K^+ currents have been described when neurons are damaged or exposed to noxious stimuli (Everill et al. 2014). Axotomy and peripheral nerve constriction have led to large downregulations of K^+ current and Kv1.4 subunit messenger RNA in DRG neurons (Kim, Choi, Rim, Cho, et al. 2002; Yang et al. 2004), which lowers the permeability of the membrane to K^+, leaving membranes hyperexcitable to subsequent stimuli, permitting spontaneous depolarization of the membrane, ectopic spike initiation and increased spontaneous firing of action potentials. Altogether, these consequences would contribute to chronic pain syndrome (Kim, Choi, Rim & Cho 2002). This hypothesis is supported by larger current I_{slow} density values in small-diameter neurons from CCI pain model rats when compared with Naïve and by Western-blot evidence regarding Kv1.3 overexpression in CCI DRG.

5.1.2.2. IS THE VOLTAGE-DEPENDENCE OF ACTIVATION IMPAIRED IN INFLAMMATORY TRASIENT PAIN?

Even though CFA rats showed a recovery in spontaneous pain and mechanical hyperalgesia to naïve values, the presented results showed that K^+ currents of CFA and Naïve derived neurons had significantly different voltage-dependence of activation, 14 days post-injury. This result indicates that the acute transient pain rats showed during the first week after the CFA injection was successful in disturbing Naïve homeostasis for the full extent of the experiment.

Chronic pathological conditions such as tissue inflammation or irritation can induce changes in the properties of somatic sensory pathways, leading to hyperalgesia and allodynia. It is described that inflammatory mediators lead to a decrease in the K^+ currents responsible for a normal resting membrane potential (Yoshimura & Groat 1999; Wells et al. 2007).Peripheral sensitization of primary afferents or changes in central synapses contribute to the increased pain sensation (Campbell & Meyer 2006; Kidd & Urban 2001).

Whole-cell voltage-clamp recordings show significant alterations in the biophysical properties of K^+ currents in small diameter DRG neurons isolated from CFA rats in comparison those from Naïve rats, obtained at the end of the behavioural tests. Since it was observed a reduction in secondary hyperalgesia assessed by vFF with the progression of the CFA model that could be translated into a recovery in their sensibility, it was postulated here that this initial state of hyperalgesia was a consequence of inflammation, which disappeared overtime. Still, there are apparent neuronal alterations, hence differences in voltage sensitivity.

Conductance results show a depolarized curve shift in both fast and steady-state currents, which translates in Kv channels being less sensitive to voltage. This means that to open a given Kv channel (of either fast or slow inactivation) of CFA small-diameter neurons, a larger stimuli would be necessary to promote to activation, resulting in a more depolarized voltage than Naïve small-diameter neurons would require. As there are also significant differences in current density values (again, regarding both fast and steady-state components), one may wonder whether it is a specific mechanism regarding Kv1.3 and Kv1.4 altered expression. In order to access this hypothesis, Western-blot in membrane enriched fractions of L3-L5 DRG must be conducted, as they are transmembrane channels. It wuld

also be advisable to conduct immunohistochemistry assays with the intention of investigating co-expression and variation levels of both Kv channels.

As previously stated, the current running through a biological membrane depends on open channel probability and duration, open channel conductance and voltage-gated channel density (Bezanilla 2005). As current conductance was already accessed by voltage-dependence of activation profiling, it is still needed to explore open channel probability and duration. This last condition was investigated by voltage-dependence of steady-state inactivation.

5.1.2.3. IS THE VOLTAGE DEPENDENCE OF STEADY-STATE INACTIVATION IMPARED IN NEUROPATHIC CHRONIC PAIN?

Steady-state inactivation curves for K^+ currents were calculated. Qualitatively, K+ currents from neurons obtained from CCI pain model rats were quite different to those obtained from Naïve ones.

Results from neurons of Naïve rats presented a double inactivation curve, suggesting the presence of two sub-populations. Analyzing steady-state inactivation fitting parameters, the first Boltzmann fit that occurs at more hyperpolarized voltages (hence termed *hyp*) refers to the I_{slow} current component and underlying Kv channels and the second Boltzmann fit that occurs at more depolarized voltages (hence termed *dep*) refers to I_{fast} current component and underlying Kv channels . As seen before (in section 4.2.3) I_{fast} K^+ currents are activated at more depolarized voltages, whereas I_{slow} K^+ currents are activated at more hyperpolarized voltages.

The cross-talk between the voltage-sensing domain and the pore domain is essential for channel activation. The first communicates with two distinct gates in the pore domain: the pore-gate in the selectivity filter and the activation-pore (Bezanilla 2005). The voltage sensor of Kv channels may experience distinct energy sceneries as it first undergoes rapid activation and subsequently finds its most stable conformation upon a prolonged depolarization (Dougherty et al. 2008). At depolarized membrane potentials, the voltage-sensor first moves quickly in order to interact with the activation-gate to open it. Then, if a depolarization is sustained, the voltage-sensor slowly drifts toward its most stable conformation. As a result, it may encounter favourable strong interactions with the pore-gate and may stabilize it in its non-conducting conformation (Elinder et al. 2001). This mechanism corresponds to the previously described C-type inactivation, which may eventually lead either to a closed-inactivated or an open-inactivated state. If the voltage-sensor interacts poorly with the pore-gate, this may still undergo rearrangements, but the lack of a strong interaction prevents stabilization of a non-conducting selectivity filter (i.e. C-type inactivation is effectively absent) (Elinder et al. 2001).

In that context, results obtained from K^+ currents of Naïve neurons, the more hyperpolarized inactivation curve refers to the characteristic of slowly inactivating Kv channels. They open at more hyperpolarized voltages, thus appearing when the prepulse is

the most hyperpolarized. As the prepulse increases, becoming gradually more depolarized, there are less K^+ channels underlying I_{slow} current, their voltage-sensor moves in order to find a more stable conformation, resulting in a non-conducting conformation. At around -50mV, a *plateau* stage is reached. This may indicate that at the same time slowly inactivating Kv channels are less probable to be found active, some A-type Kv channels are becoming active. These activate at more depolarized voltages and the current now passing through them elevates the decreasing current of slowly inactivating Kv channels, creating that *plateau* stage. As the protocol reaches even more depolarized voltages, A-type Kv channels also become more and more inactive, creating the second Boltzmann behaviour.

CCI results are very similar to Naïve, but the second Boltzmann fit (*dep* – the one associated with I_{fast} current and underlying Kv channels) is much less pronounced. These findings corroborate with current density obtained in subtracted whole-cell currents of CCI neurons. As the A-type Kv channels appear to be less expressed in CCI (section 4.3.1), their subpopulation is unpronounced in this protocol. It is also needed to address the voltage slope of the first Boltzmann fit (*hyp* – the one associated with I_{slow} current and underlying Kv channels) of CCI voltage-dependence of steady-state inactivation. The curve obtained from K^+ currents of CCI neurons show a larger voltage slope than those found in Naïve neurons. *This indicates that in the CCI pain model, the slowly inactivating currents, at more depolarized voltages, depict more channels available for activation.*

Lastly, CCI neurons showed a persistent/non-inactivating current, also corroborating the hypothesis of a higher expression of Kv channels responsible for I_{slow} current component in CCI neurons.

5.1.2.4. IS THE VOLTAGE DEPENDENCE OF STEADY-STATE INACTIVATION IMPARED IN INFLAMMATORY TRANSIENT PAIN?

Voltage-dependence of steady-state inactivation curve of K^+ currents from CFA neurons is not characterized by a sum of two Boltzmann functions. When compared with Naïve curve, it is visible the disappearance of the second Boltzmann fit. This observation, following the previous rationale, indicates that the A-type Kv channel sub-population is much less active than in Naïve conditions. In addition, this finding corroborates the poor expression or even disappearance of A-type current in whole-cell current traces and lowered current density values.

5.1.3. ARE KV CHANNELS BEING RECRUITED FROM DRG TO SCIATIC NERVE AS CONSEQUENCE OF NERVE HYPEREXCITABILITY?

Fibers of the same neurons conduct more slowly in the dorsal root than the peripheral nerve (Waddell et al. 1989). Following axonal injury sensory axons become hyperexcitable, which maintains neuropathic pain (Han et al., 2000). The K^+ currents mediated by Kv1 channels are reduced in chronic pain condition, when measured at the soma of small diameter DRG neurons (Rasband et al. 2001; Kim et al. 2002; K Ishikawa et al. 1999), resulting on the loss of the neuronal 'break' of excitability. There has been, however, much less focus on the distribution and function of Kv1 channels within the axon following peripheral nerve injury.

A recent study (Calvo et al. 2016) has found major changes in Kv1 channels subunit composition and distribution within the DRG axon following traumatic nerve injury. In contrast to the soma in which Kv1 channels expression is reduced, they found an increased availability of Kv1 channels and altered subunit composition. They conclude stating that this finding appears to fulfil an adaptive role in suppressing excessive excitability in primary afferents during neuropathic pain following peripheral nerve injury.

Western-blot assays in the present report have shown an increased expression of Kv1.3 which corroborates with the functional increase of Islow; also, a tendency to increased

or unchanged expression Kv1.4 that somehow contradicts a marked decrease of I_{fast}. Such dynamics may be dictating a yet more relevant one at the sciatic nerve which must be followed in future research. These results are corroborated by Calvo et. al.'s aforementioned findings (Calvo et al. 2016). An hyperexcitable axon conducts faster and has a differential Kv expression when compared with the soma.

Our results and reports such as Calvo et. al's, suggest that the DRG may act as a 'buffer unit' of channels of the operant axonic portion, the sciatic nerve. Hence a decrease of a certain current at the DRGs, such as the I_{fast} and the underlying channels expression, may just be happening as a consequence of the effort to enable larger functional availability of channels at the axon (and vice versa).

Still, it is not very linear whether the variation expression of these isoforms is due to a mobilization of Kv channels from the soma to the axon or not. Once again, Western-blot assays were performed using whole-sciatic nerve lysate, instead of using plasma-enriched proximal axon preparations. As a future direction, it would be interesting to also conduct immunohistochemistry assays in proximal sciatic nerve. Also, current clamp recordings should be done in sciatic nerve of Naïve and pain model rats in order to access information such as the firing pattern.

Conclusions

The present work revealed some insights of the physiopathology inflammatory and neuropathic chronic pain. Briefly, chronic pain model rats exhibited an altered behaviour in comparison to their controls. Furthermore, it was observed an impaired function and expression of K^+ currents and underlying Kv channels in small-diameter DRG neurons following such pain models:

- ✓ Inflammatory and Neuropathic conditions share an underlying mechanism regarding the reduction of I_{fast};
- ✓ Inflammatory pain shows a specific underlying mechanism regarding a depolarized shift in the activation profile of the I_{fast} current component, which is in accordance with previous studies;
- ✓ Neuropathic chronic pain shows a specific underlying mechanism regarding the increase of the I_{slow} current component, which is a new finding in the context of chronic pain;
- ✓ Kv1.3 over-expression may be responsible for the increase in I_{slow} K^+ current.

Altogether, results account for the increase of neuroexcitability in both chronic pain models, which is associated with the exacerbation of excitation that is not proportional to the strength of the external stimulation.

Importantly, this study identified two channels as key effectors in the alteration of neuroexcitability: Kv1.3 and Kv1.4, hence attributing a role of therapeutic targets.

Future Directions

- Current clamp recordings by in vivo recordings from pain rat models. Current clamp would refine the study of cell excitability, and extracellular recording would open up the study to the repercussions of the observed neuroexcitability modifications onto synaptic performance;
- It would be advantageous to study more time periods of CFA pain model rats in order to characterize Kv channels in acute pain and learn to distinguish them to what has been characterized in this study;
- Also regarding the CFA pain model, it would be advisable to restructure the protocol of inflammatory chronic pain induction by introducing a priming step;
- Painful diabetic neuropathy should also be restructured. STZ should be dissolved in the appropriate vehicle and the duration of the study should be readjusted to 8 weeks (since painful neuropathy is described to begin 4 weeks after diabetes establishment);
- In relation to Kv1.3 and Kv1.4 expression, it would be useful to use plasma-membrane enriched preparations in Western-blot assays to correlate expression pattern with electrophysiology data. It would also be advisable to run immunohistochemistry and immunocytochemistry assays regarding both Kv channels, in order to access their precise localization and expression patterns.

REFERENCES

Abdulla, F.A. & Smith, P.A., 2001. Axotomy- and autotomy-induced changes in Ca2+ and K+ channel currents of rat dorsal root ganglion neurons. *J Neurophysiol*, 85(2), pp.644–658. Available at: http://www.ncbi.nlm.nih.gov/pubmed/11160500%5Cnhttp://jn.physiology.org/content/85/2/644.full.pdf.

Abrahamsen, B., 2014. The Cell and Molecular Basis of Mechanical, Cold, and Inflammatory Pain. , 702(2008).

Abrahamsen, B. et al., 2008. The cell and molecular basis of mechanical, cold, and inflammatory pain. *Science (New York, N.Y.)*, 321(5889), pp.702–705.

Armstrong, C.M., 2003. Voltage-Gated K Channels. *Sci. STKE*, 2003(188), p.re10-. Available at: http://stke.sciencemag.org/cgi/content/abstract/sigtrans%5Cn2003/188/re10.

Armstrong, C.M. & Hille, B., 1998. Voltage-Gated Ion Channels Review and Electrical Excitability. *Neuron*, 20, pp.371–380.

Attal, N. et al., 1990. Further evidence for “pain-related” behaviours in a model of unilateral peripheral mononeuropathy. *Pain*, 41(2), pp.235–251.

Austin, P.J., Wu, A. & Moalem-Taylor, G., 2012. Chronic constriction of the sciatic nerve and pain hypersensitivity testing in rats. *Journal of visualized experiments : JoVE*, (61), pp.1–6. Available at: http://www.pubmedcentral.nih.gov/articlerender.fcgi?artid=3399467&tool=pmcentrez&rendertype=abstract.

Axelrod, F.B. & Hilz, M.J., 2003. Inherited autonomic neuropathies. *Seminars in neurology*, 23(4), pp.381–390.

Azevedo, F. et al., 2012. Epidemiology of Chronic Pain: A Population-Based Nationwide Study on Its Prevalence, Characteristics and Associated Disability in Portugal. , 13(8), pp.773–783.

Baron, R., 2006. Mechanisms of disease: neuropathic pain - a clinical perspective. *Nature*

clinical practice. Neurology, 2(2), pp.95–106.

Barrett, J.E., 2015. The pain of pain: Challenges of animal behavior models. *European Journal of Pharmacology*, 753, pp.183–190. Available at: http://dx.doi.org/10.1016/j.ejphar.2014.11.046.

Basbaum, A.I. et al., 2009. Cellular and Molecular Mechanisms of Pain. *Cell*, 139(2), pp.267–284.

Beekwilder, J.P. et al., 2003. Kv1. 1 Channels of Dorsal Root Ganglion Neurons Are Inhibited byn-Butyl-p-aminobenzoate, a Promising Anesthetic for the Treatment of Chronic Pain. *Journal of Pharmacology and Experimental Therapeutics*, 304(2), pp.531–538.

Bezanilla, F., 2005. Voltage-gated ion channels. *IEEE Transactions on Nanobioscience*, 4(1), pp.34–48.

Borzan, J. et al., 2010. Effects of soy diet on inflammation-induced primary and secondary hyperalgesia in rat. *European journal of pain (London, England)*, 14(8), pp.792–798.

Bosma, M.M. & Hille, B., 1992. Electrophysiological properties of a cell line of the gonadotrope lineage. *Endocrinology*, 130(6), pp.3411–3420.

Brown, D.A. & Adams, P.R., 1980. Muscarinic suppression of a novel voltage-sensitive K+ current in a vertebrate neurone. *Nature*, 283(5748), pp.673–676.

Brown, D.A. & Passmore, G.M., 2009. Neural KCNQ (Kv7) channels. *British journal of pharmacology*, 156(8), pp.1185–1195.

Calvo, M. et al., 2016. Altered potassium channel distribution and composition in myelinated axons suppresses hyperexcitability following injury. *eLife*, 5(APRIL2016), pp.1–26.

Camacho, J., 2006. Ether a go-go potassium channels and cancer. *Cancer letters*, 233(1), pp.1–9.

Campbell, J.N. & LaMotte, R.H., 1983. Latency to detection of first pain. *Brain research*, 266(2), pp.203–208.

Campbell, J.N. & Meyer, R.A., 2006. Mechanisms of Neuropathic Pain Review. *Neuron*, 52(November), pp.77–92. Available at:

http://www.pubmedcentral.nih.gov/articlerender.fcgi?artid=1810425&tool=pmcentrez&rendertype=abstract.

Cao, X.-H. et al., 2011. Reduction in Voltage-Gated K+ Channel Activity in Primary Sensory Neurons in Painful Diabetic Neuropathy: Role of Brain- Derived Neurotrophic Factor. *J Neurochem.*, 114(5), pp.1460–1475.

Carozzi, V.A. et al., 2013. Bortezomib-Induced Painful Peripheral Neuropathy: An Electrophysiological, Behavioral, Morphological and Mechanistic Study in the Mouse. *PLoS ONE*, 8(9), pp.1–19.

Choe, S., 2002. Potassium channel structures. *Nat Rev Neurosci*, 3(2), pp.115–121. Available at: http://dx.doi.org/10.1038/nrn727.

Coetzee, W.A. et al., 1999. Molecular diversity of K+ channels. *Annals of the New York Academy of Sciences*, 868, pp.233–285.

Cooper, E.C. et al., 1998. Presynaptic Localization of Kv1 . 4-Containing A-Type Potassium Channels Near Excitatory Synapses in the Hippocampus. , 18(3), pp.965–974.

Decosterd, I. & Woolf, C.J., 2000. Spared nerve injury: An animal model of persistent peripheral neuropathic pain. *Pain*, 87(2), pp.149–158.

Djouhri, L., Bleazard, L. & Lawson, S.N., 1998. Association of somatic action potential shape with sensory receptive properties in guinea-pig dorsal root ganglion neurones. *The Journal of Physiology*, 513(3), pp.857–872. Available at: http://dx.doi.org/10.1111/j.1469-7793.1998.857ba.x.

Djouhri, L. & Lawson, S.N., 2004. A??-fiber nociceptive primary afferent neurons: A review of incidence and properties in relation to other afferent A-fiber neurons in mammals. *Brain Research Reviews*, 46(2), pp.131–145.

Dougherty, K., Santiago-Castillo, J.A. De & Covarrubias, M., 2008. Gating charge immobilization in Kv4 . 2 channels : the basis of closed-state inactivation .

Doyle, D.A. et al., 1998. The structure of the potassium channel: molecular basis of K+ conduction and selectivity. *Science (New York, N.Y.)*, 280(5360), pp.69–77.

Du, X. & Gamper, N., 2013. Potassium channels in peripheral pain pathways: expression, function and therapeutic potential. *Current neuropharmacology*, 11(6), pp.621–40.

Elinder, F., Männikkö, R. & Larsson, H.P., 2001. S4 Charges Move Close to Residues in

the Pore Domain during Activation in a K Channel. , 118(July).

Everill, B. et al., 2014. Reduction in Potassium Currents in Identified Cutaneous Afferent Dorsal Root Ganglion Neurons After Axotomy Reduction in Potassium Currents in Identified Cutaneous Afferent Dorsal Root Ganglion Neurons After Axotomy. , (Devor 1994), pp.700–708.

Everill, B., Rizzo, M.A. & Kocsis, J.D., 1998. Morphologically Identified Cutaneous Afferent DRG Neurons Express Three Different Potassium Currents in Varying Proportions. *Journal of neurophysiology*, 79(4), pp.1814–1824.

Fan, L. et al., 2014. Impaired neuropathic pain and preserved acute pain in rats overexpressing voltage-gated potassium channel subunit Kv1.2 in primary afferent neurons. *Molecular pain*, 10(1), p.8. Available at: http://www.pubmedcentral.nih.gov/articlerender.fcgi?artid=3909300&tool=pmcentrez&rendertype=abstract.

Fein, A., 2012. Nociceptors and the perception of pain. *Nociceptors and the perception of pain*, (February), pp.5–7. Available at: http://cell.uchc.edu/pdf/fein/nociceptors_fein_2012.pdf.

Fields, H.L., 1987. Analgesic drugs. *Pain*, 1, p.272.

Finnerup, N.B. et al., 2007. An Evidence-Based Algorithm for the Treatment of Neuropathic Pain. *Medscape General Medicine*, 9(2), p.36.

Frank, H.Y. et al., 2005. Overview of molecular relationships in the voltage-gated ion channel superfamily. *Pharmacological reviews*, 57(4), pp.387–395.

Fukuoka, T. et al., 2012. Re-evaluation of the phenotypic changes in L4 dorsal root ganglion neurons after L5 spinal nerve ligation. *Pain*, 153(1).

Grizel, A. V, Glukhov, G.S. & Sokolova, O.S., 2014. Mechanisms of Activation of Voltage-Gated Potassium Channels. , 6(23), pp.10–26.

Guan, G. et al., 2005. Estrogenic effect on swelling and monocytic receptor expression in an arthritic temporomandibular joint model. *The Journal of steroid biochemistry and molecular biology*, 97(3), pp.241–250.

Gutman, G.A. et al., 2005. International Union of Pharmacology. LIII. Nomenclature and molecular relationships of voltage-gated potassium channels. *Pharmacological*

reviews, 57(4), pp.473–508.

Hao, J. et al., 2013. Kv1.1 channels act as mechanical brake in the senses of touch and pain. *Neuron*, 77(5), pp.899–914.

Hart, B.L., 1988. Biological basis of the behavior of sick animals. *Neuroscience & Biobehavioral Reviews*, 12(2), pp.123–137. Available at: http://www.sciencedirect.com/science/article/pii/S0149763488800046.

Helms, J.E. & Barone, C.P., 2008. Physiology and Treatment of Pain. *Crit Care Nurse*, 28(6), pp.38–49.

Heng, L.J. et al., 2015. Docosahexaenoic acid inhibits mechanical allodynia and thermal hyperalgesia in diabetic rats by decreasing the excitability of DRG neurons. *Experimental Neurology*, 271, pp.291–300. Available at: http://dx.doi.org/10.1016/j.expneurol.2015.06.022.

Hille, B., 2001. Ion Channel Excitable Membranes. *Book*, pp.1–37.

Hodgkin, A.L. & Huxley, A.F., 1952. A quantitative description of membrane current and its application to conduction and excitation in nerve. *The Journal of Physiology*, 117(4), pp.500–544.

Holden, A. V & Winlow, W., 1984. *The Neurobiology of Pain: Symposium of the Northern Neurobiology Group, Held at Leeds on 18 April, 1983*, Manchester University Press.

Horn, R., 2005. How ion channels sense membrane potential. *Proceedings of the National Academy of Sciences of the United States of America*, 102(14), pp.4929–4930.

Ishikawa, K. et al., 1999. Changes in expression of voltage-gated potassium channels in dorsal root ganglion neurons following axotomy. *Muscle & nerve*, 22(4), pp.502–507.

Ishikawa, K. et al., 1999. Changes in expression of voltage-gated potassium channels in dorsal root ganglion neurons following axotomy. *Muscle & nerve*, 22(April), pp.502–507.

Iyer, S. & Tanenberg, R.J., 2013. Pharmacologic management of diabetic peripheral neuropathic pain. *Expert opinion on pharmacotherapy*, 14(13), pp.1765–1775.

Julius, D., 2001. Molecular mechanisms of nociception . *Nature*, 413(September),

pp.203–210.

Julius, D. & Basbaum, A.I., 2001. Molecular mechanisms of nociception. *Nature*, 413(6852), pp.203–210.

Kajander, K.C., Pollock, C.H. & Berg, H., 1996. Evaluation of hind paw position in rats during chronic constriction injury (CCI) produced with different suture materials. *Somatosensory & motor research*, 13(2), pp.95–101. Available at: http://www.ncbi.nlm.nih.gov/pubmed/8844958.

Kendall, N.A.S., 1999. Psychosocial approaches to the prevention of chronic pain: the low back paradigm. *Best Practice & Research Clinical Rheumatology*, 13(3), pp.545–554.

Kidd, B.L. & Urban, L.A., 2001. Mechanisms of Inflammatory Pain. , 87(1).

Kim, D.S., Choi, J.O., Rim, H.D. & Cho, H.J., 2002. Downregulation of voltage-gated potassium channel $α$ gene expression in dorsal root ganglia following chronic constriction injury of the rat sciatic nerve. *Molecular brain research*, 105(1), pp.146–152.

Kim, D.S., Choi, J.O., Rim, H.D., Cho, H.J., et al., 2002. Downregulation of voltage-gated potassium channel alpha gene expression in dorsal root ganglia following chronic constriction injury of the rat sciatic nerve. *Molecular Brain Research*, 105(1–2), pp.146–152. Available at: http://ovidsp.ovid.com/ovidweb.cgi?T=JS&PAGE=reference&D=emed5&NEWS=N&AN=2002388095%5Cnhttp://ovidsp.ovid.com/ovidweb.cgi?T=JS&PAGE=reference&D=med4&NEWS=N&AN=12399117.

von Kitzing, E., Jonas, P. & Sakmann, B., 1994. Europepmc_Citation. *Research in Veterinary Science*, 30(3), pp.364–367.

Koo, S.T. et al., 2013. The effects of pressure on arthritic knees in a rat model of CFA-induced arthritis. *Pain Physician*, 16(2), pp.95–102. Available at: http://www.ncbi.nlm.nih.gov/pubmed/23511695%5Cnhttp://www.scopus.com/inward/record.url?eid=2-s2.0-84875281603&partnerID=tZOtx3y1.

Kostyuk, P.G. et al., 1981. IONIC CURRENTS IN THE SOMATIC MEMBRANE OF RAT DORSAL ROOT. , 6(12).

Lepine, J.-P. & Briley, M., 2004. The epidemiology of pain in depression. *Human psychopharmacology*, 19 Suppl 1, pp.S3-7.

Leung, Y.-M., 2012. Involvement of C-type inactivation gating in the actions of voltage-gated K+ channel inhibitors. *Pharmacology & therapeutics*, 133(2), pp.151–158.

Li, L. et al., 2015. Exogenous brain-derived neurotrophic factor relieves pain symptoms of diabetic rats by reducing excitability of dorsal root ganglion neurons. *International Journal of Neuroscience*, 7454(November), pp.1–10. Available at: http://www.tandfonline.com/doi/full/10.3109/00207454.2015.1057725.

Long, S.B., Campbell, E.B. & Mackinnon, R., 2005. Crystal structure of a mammalian voltage-dependent Shaker family K+ channel. *Science (New York, N.Y.)*, 309(5736), pp.897–903.

Ludwig, M. & Pittman, Q.J., 2003. Talking back: dendritic neurotransmitter release. *Trends in neurosciences*, 26(5), pp.255–261.

Lujan, R., 2010. Organisation of potassium channels on the neuronal surface. *Journal of chemical neuroanatomy*, 40(1), pp.1–20.

Margrie, T.W. & Urban, N., 2007. Dendrites as transmitters. *Dendrites*, p.401.

Mathie, A., Wooltorton, J.R. & Watkins, C.S., 1998. Voltage-activated potassium channels in mammalian neurons and their block by novel pharmacological agents. *General pharmacology*, 30(1), pp.13–24.

Matsuka, Y. et al., 2001. Concurrent release of ATP and substance P within guinea pig trigeminal ganglia in vivo. *Brain research*, 915(2), pp.248–255.

McCaffery, M. & Beebe, a., 1989. Pain: Clinical manual for nursing practice. The Numeric Pain Rating Scale. *Pain*, 0, p.1989. Available at: http://www.rehabmeasures.org/PDF Library/Numeric Pain Rating Scale Instructions.pdf.

Miller, C., 2000. An overview of the potassium channel family. *Genome biology*, 1(4), p.REVIEWS0004. Available at: http://www.pubmedcentral.nih.gov/articlerender.fcgi?artid=138870&tool=pmcentrez&rendertype=abstract%5Cnhttp://www.ncbi.nlm.nih.gov/pubmed/11178249%5Cnhttp://www.pubmedcentral.nih.gov/articlerender.fcgi?artid=PMC138870.

Milton, J., 2013. Caring for patients with chronic pain: pearls and pitfalls. *The Journal*, 113(8), pp.620–627.

Minett, M.S., Eijkelkamp, N. & Wood, J.N., 2014. Significant determinants of mouse pain behaviour. *PLoS ONE*, 9(8).

Mishra, P. & Narayanan, R., 2014. High-conductance states and A-type K+ channels are potential regulators of the conductance-current balance triggered by HCN channels. *Journal of neurophysiology*, 113(1), pp.23–43. Available at: http://www.ncbi.nlm.nih.gov/pubmed/25231614.

Mishra, S.K. et al., 2010. TRPV1-lineage neurons are required for thermal sensation. *The EMBO Journal*, 30(3), pp.582–593. Available at: http://dx.doi.org/10.1038/emboj.2010.325.

Misonou, H., 2010. Homeostatic regulation of neuronal excitability by K(+) channels in normal and diseased brains. *The Neuroscientist : a review journal bringing neurobiology, neurology and psychiatry*, 16(1), pp.51–64.

Mogil, J.S., 2009. Animal models of pain: progress and challenges. *Nature reviews. Neuroscience*, 10(4), pp.283–294.

Mogil, J.S., Davis, K.D. & Derbyshire, S.W., 2010. The necessity of animal models in pain research. *Pain*, 151(1), pp.12–17.

Nashmi, R. & Fehlings, M.G., 2001. Mechanisms of axonal dysfunction after spinal cord injury: with an emphasis on the role of voltage-gated potassium channels. *Brain research. Brain research reviews*, 38(1–2), pp.165–191.

Nicholls, J. G., Martin, A. R., & Wallace, B.G., 1992. *From Neuron to Brain: A cellular and molecular approach to the function of the nervous system* 3rd ed., Sunderland (MA): Sinauer Associates.

Park, S.Y. et al., 2003. Downregulation of voltage-gated potassium channel alpha gene expression by axotomy and neurotrophins in rat dorsal root ganglia. *Molecules and cells*, 16(2), pp.256–259.

Pischalnikova, A. V & Sokolova, O.S., 2009. The domain and conformational organization in potassium voltage-gated ion channels. *Journal of neuroimmune pharmacology : the official journal of the Society on NeuroImmune Pharmacology*, 4(1), pp.71–82.

Purves D, Augustine GJ, Fitzpatrick D, et al., 2001. *Neuroscience* 2nd ed. Neuroscience, ed., Sunderland (MA): Sinauer Associates. Available at: https://www.ncbi.nlm.nih.gov/books/NBK10965/.

Raj, P.P. et al., 2007. Taxonomy and classification of pain. The hand book of chronic pain.

Rasband, M.N. et al., 2001. Distinct potassium channels on pain-sensing neurons. *Proceedings of the National Academy of Sciences of the United States of America*, 98(23), pp.13373–13378.

Reichling, D.B. & Levine, J.D., 2010. Critical role of nociceptor plasticity in chronic pain. , 32(12), pp.611–618.

Ren, K. & Dubner, R., 1999. Inflammatory Models of Pain and Hyperalgesia. *ILAR journal / National Research Council, Institute of Laboratory Animal Resources*, 40(3), pp.111–118. Available at: http://eutils.ncbi.nlm.nih.gov/entrez/eutils/elink.fcgi?dbfrom=pubmed&id=11406689&retmode=ref&cmd=prlinks%5Cnpapers3://publication/uuid/050C516D-F7BF-4720-B196-F91BEE4A0385.

Robbins, J., 2001. KCNQ potassium channels: physiology, pathophysiology, and pharmacology. *Pharmacology & therapeutics*, 90(1), pp.1–19.

Rose, K. et al., 2011. Transcriptional repression of the M channel subunit Kv7.2 in chronic nerve injury. *Pain*, 152(4), pp.742–754. Available at: http://dx.doi.org/10.1016/j.pain.2010.12.028.

Russo MD, C.M. & Brose MD, W.G., 1998. Chronic pain. *Annual review of medicine*, 49(1), pp.123–133.

Sauer, B., 1987. Functional Expression of the cre-lox Site-Specific Recombination System in the Yeast Saccharomyces cerevisiae. , 7(6), pp.2087–2096.

Schaible, H.-G., 2007. Peripheral and central mechanisms of pain generation. *Analgesia*, pp.3–28.

Serrão, J., 2015. Validation of voltage-gated sodium channels from dorsal root ganglia neurons as a pharmacological target for the treatment of Chronic pain.

Sherrington, C.S., 1906. The integrative action of the nervous system. *Scribner*.

Sigworth, F.J., 1994. Voltage gating of ion channels. *Quarterly reviews of biophysics*,

27(1), pp.1–40.

Sik Nam, J. et al., 2014. Effects of Nefopam on Streptozotocin-Induced Diabetic Neuropathic Pain in Rats. *Korean J Pain*, 27(4), pp.326–333. Available at: http://dx.doi.org/10.3344/kjp.2014.27.4.326.

Southan, a P. & Robertson, B., 2000. Electrophysiological characterization of voltage-gated K(+) currents in cerebellar basket and purkinje cells: Kv1 and Kv3 channel subfamilies are present in basket cell nerve terminals. *The Journal of neuroscience : the official journal of the Society for Neuroscience*, 20(1), pp.114–122.

Spears, R. et al., 2005. Temporal changes in inflammatory mediator concentrations in an adjuvant model of temporomandibular joint inflammation. *Journal of orofacial pain*, 19(1), pp.34–40.

Takeda, M. et al., 2011. Potassium channels as a potential therapeutic target for trigeminal neuropathic and inflammatory pain. *Mol Pain*, 7(5), pp.1–8. Available at: http://www.molecularpain.com/content/7/1/5.

Tesfaye, S. & Kempler, P., 2005. Painful diabetic neuropathy. *Diabetologia*, 48(5), pp.805–807.

Tsantoulas, C. & McMahon, S.B., 2014. Opening paths to novel analgesics: The role of potassium channels in chronic pain. *Trends in Neurosciences*, 37(3), pp.146–158. Available at: http://dx.doi.org/10.1016/j.tins.2013.12.002.

Turk, D.C., Dworkin, R.H. & others, 2004. What should be the core outcomes in chronic pain clinical trials? *Arthritis research and therapy*, 6, pp.151–173.

Vydyanathan, A. et al., 2005. A-Type Voltage-Gated K ƨ Currents Influence Firing Properties of Isolectin B 4 -Positive But Not Isolectin B 4 -Negative Primary Sensory Neurons. , pp.3401–3409.

Waddell, P.J., Lawson, S.N. & McCarthy, P.W., 1989. Conduction velocity changes along the processes of rat primary sensory neurons. *Neuroscience*, 30(3), pp.577–584.

Wang, Q. et al., 1996. Positional cloning of a novel potassium channel gene: KVLQT1 mutations cause cardiac arrhythmias. *Nature genetics*, 12(1), pp.17–23.

Wattiez, A. et al., 2012. Rodent Models of Painful Diabetic Neuropathy : What Can We Learn from Them ? *Diabetes & Metabolism*, pp.5–8.

Waxman, S.G. & Zamponi, G.W., 2014. Regulating excitability of peripheral afferents: emerging ion channel targets. *Nature neuroscience*, 17(2), pp.153–163. Available at: http://dx.doi.org/10.1038/nn.3602.

Wells, J.E. et al., 2007. Kv1.4 Subunit Expression is Decreased in Neurons of Painful Human Pulp. *Journal of Endodontics*, 33(7), pp.827–829.

Wu, K.K. & Huan, Y., 2008. Streptozotocin-induced diabetic models in mice and rats. *Current Protocols in Pharmacology*, (SUPPL. 40), pp.1–14.

Wu, R.L. & Barish, M.E., 1992. Two pharmacologically and kinetically distinct transient potassium currents in cultured embryonic mouse hippocampal neurons. *The Journal of neuroscience : the official journal of the Society for Neuroscience*, 12(6), pp.2235–2246.

Wulff, H. & Castle, N., 2009. Voltage-gated potassium channels as therapeutic targets. *Nature Reviews Drug Discovery*, 8(12), pp.982–1001. Available at: http://www.nature.com/nrd/journal/vaop/ncurrent/full/nrd2983.html.

Yang, E.-K. et al., 2004. Altered expression of potassium channel subunit mRNA and $α$-dendrotoxin sensitivity of potassium currents in rat dorsal root ganglion neurons after axotomy. *Neuroscience*, 123(4), pp.867–874.

Yellen, G., 2002. The voltage-gated potassium channels and their relatives. *Nature*, 419(6902), pp.35–42.

Yoshimura, N. & Groat, W.C. De, 1999. Increased Excitability of Afferent Neurons Innervating Rat Urinary Bladder after Chronic Bladder Inflammation. , 19(11), pp.4644–4653.

Zhang, J.M. et al., 1997. Axotomy increases the excitability of dorsal root ganglion cells with unmyelinated axons. *Journal of neurophysiology*, 78, pp.2790–2794.

Zheng, Q. et al., 2013. Suppression of KCNQ/M (Kv7) potassium channels in dorsal root ganglion neurons contributes to the development of bone cancer pain in a rat model. *Pain*, 154(3), pp.434–448.